Gastroenterology 2021;160:1345–1358

Extracellular Vesicle Analysis Allows for Identification of Invasive IPMN

Katherine S. Yang,[1] Debora Ciprani,[2] Aileen O'Shea,[1,3] Andrew S. Liss,[2] Robert Yang,[1] Sarah Fletcher-Mercaldo,[3] Mari Mino-Kenudson,[4] Carlos Fernández-del Castillo,[2] and Ralph Weissleder[1,3,5]

[1]Center for Systems Biology, Massachusetts General Hospital, Boston, Massachusetts; [2]Department of Surgery, Massachusetts General Hospital, Boston, Massachusetts; [3]Department of Radiology, Massachusetts General Hospital, Boston, Massachusetts; [4]Department of Pathology, Massachusetts General Hospital, Boston, Massachusetts; and [5]Department of Systems Biology, Harvard Medical School, Boston, Massachusetts

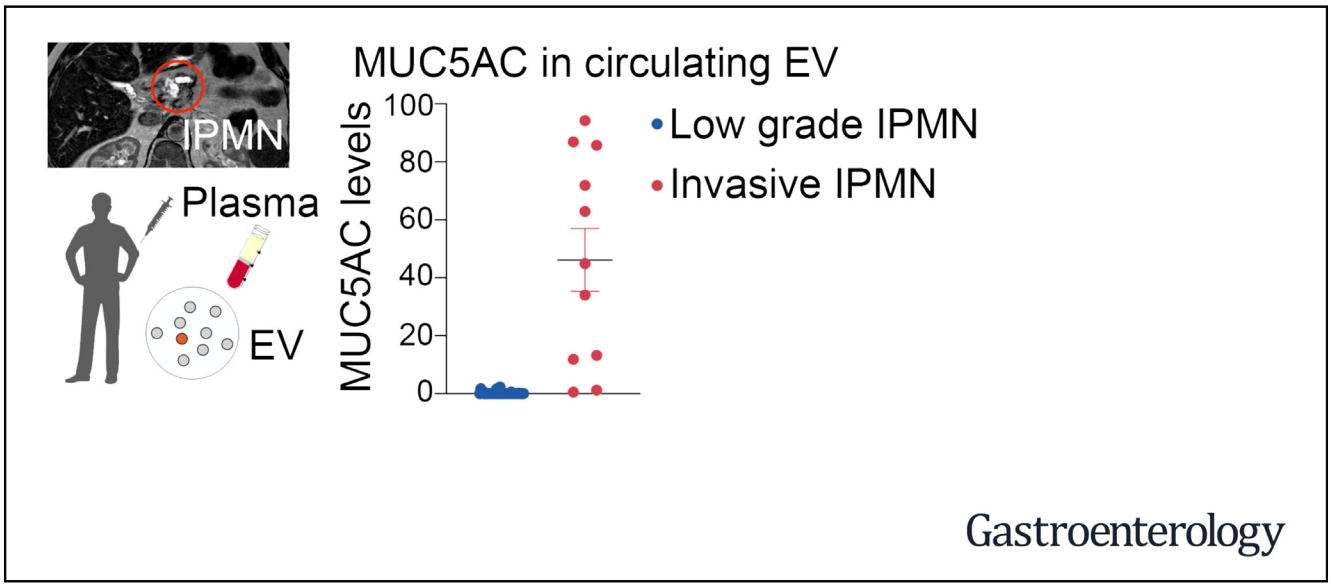

See editorial on page 1016.

BACKGROUND AND AIMS: Advances in cross-sectional imaging have resulted in increased detection of intraductal papillary mucinous neoplasms (IPMNs), and their management remains controversial. At present, there is no reliable noninvasive method to distinguish between indolent and high risk IPMNs. We performed extracellular vesicle (EV) analysis to identify markers of malignancy in an attempt to better stratify these lesions. **METHODS:** Using a novel ultrasensitive digital extracellular vesicle screening technique (DEST), we measured putative biomarkers of malignancy (MUC1, MUC2, MUC4, MUC5AC, MUC6, Das-1, STMN1, TSP1, TSP2, EGFR, EpCAM, GPC1, WNT-2, EphA2, S100A4, PSCA, MUC13, ZEB1, PLEC1, HOOK1, PTPN6, and FBN1) in EV from patient-derived cell lines and then on circulating EV obtained from peripheral blood drawn from patients with IPMNs. We enrolled a total of 133 patients in two separate cohorts: a clinical discovery cohort (n = 86) and a validation cohort (n = 47). **RESULTS:** From 16 validated EV proteins in plasma samples collected from the discovery cohort, only MUC5AC showed significantly higher levels in high-grade lesions. Of the 11 patients with invasive IPMN (inv/HG), 9 had high MUC5AC expression in plasma EV of the 11 patients with high-grade dysplasia alone, only 1 had high MUC5AC expression (sensitivity of 82%, specificity of 100%). These findings were corroborated in a separate validation cohort. The addition of MUC5AC as a biomarker to imaging and *high-risk stigmata* allowed detection of all cases requiring surgery, whereas imaging and *high-risk stigmata* alone would have missed 5 of 14 cases (36%). **CONCLUSIONS:** MUC5AC in circulating EV can predict the presence of invasive carcinoma within IPMN. This approach has the potential to improve the management and follow-up of patients with IPMN including avoiding unnecessary surgery.

Keywords: Pancreatic cancer; IPMN; Precancer; Early detection; Exosome.

The detection of intraductal papillary mucinous neoplasms (IPMNs) is rising due to the increasing use and improved quality of cross-sectional imaging.[1] These

Abbreviations used in this paper: **AUC, area under the curve; DEST, digital extracellular vesicle screening technique; EGFR, epidermal growth factor receptor; ELISA, enzyme-linked immunosorbent assay; EpCAM, epithelial cell adhesion molecule; EV, extracellular vesicle; GPC1, glypican 1; HG, high grade; IPMN, intraductal papillary mucinous neoplasm; inv/HG, invasive high grade; LG, low grade; MUC1, mucin 1; MUC5AC, mucin 5AC, oligomeric mucus/gel-forming; PBS, phosphate-buffered saline; PDAC, pancreatic ductal adenocarcinoma; PDX, patient-derived xenograft; ROC, receiver operating characteristic; TSP1, thrombospondin-1; TSP2, thrombospondin-2; WNT-2, wingless-type MMTV integration site family, member 2.**

Most current article

0016-5085/$36.00
https://doi.org/10.1053/j.gastro.2020.11.046

WHAT YOU NEED TO KNOW

BACKGROUND AND CONTEXT

Increasing detection of intraductal papillary mucinous neoplasms (IPMNs) from cross-sectional imaging is a problem for clinicians since these patients will require prolonged surveillance. A non-invasive method for the distinction of indolent from invasive subtypes is an unmet clinical need.

NEW FINDINGS

Blood based analysis of extracellular vesicles (EV) permits the distinction of invasive IPMNs from low grade and non-invasive subtypes.

LIMITATIONS

133 patients were examined in this study, of which 83 ultimately underwent surgical resection with histopathologic correlation. Confirmation of our study findings will require studies in larger cohorts inclusive of both surgical candidates and non-operative candidates undergoing surveillance.

IMPACT

Our results show that MUC5AC EV profiling reliably identifies patients with invasive IPMN. When combined with imaging and clinical findings, the DEST method has the potential to transform IPMN/early PDAC cancer detection and surgical evaluation.

cystic neoplasms have been shown to evolve from low-grade (LG) dysplasia to high-grade (HG) dysplasia to invasive carcinoma (inv/HG). This pathway of progression is believed to account for up to a quarter of all pancreatic cancers.[2] The timing and frequency of malignant progression is unknown, and therefore, the management of patients with some forms of IPMN, in particular branch-duct IPMN, remains controversial.[3–7] This is in large part because current laboratory, endoscopic, cytologic, and imaging technologies are unable to reliably distinguish between low-risk and high-risk IPMN. Although analysis of cyst fluid has shown some promise,[8] it requires repeat interventional endoscopy, and the amounts of aspirated fluid in IPMN can be too small for analysis.

Even though most IPMNs will not progress, there is no reliable way to predict which ones will, and currently, most of these patients undergo periodic surveillance with magnetic resonance imaging or computed tomography. Some guidelines recommend stopping surveillance at 5 or 10 years, but other studies have shown that progression can occur beyond this time frame,[9] and therefore, lifelong surveillance may be required.[5] This implies an enormous cost given the number of patients with incidentally discovered pancreatic cysts and that incidence increases with age.[10]

We hypothesize that analysis of circulating extracellular vesicles (EVs) originating from (pre)malignant cells represents an opportunity for analyzing IPMNs and early pancreatic cancers. Several challenges exist, including the absence of known biomarkers that can identify high-risk IPMN. Indeed, a recent consensus conference concluded that "there are no available DNA, RNA or protein biomarkers in blood for clinical use to differentiate pancreatic cyst type or identify high grade dysplasia or cancer."[6] We thus first set out to identify and measure EV concentrations of known protein biomarkers that have been associated with pancreatic cancer in the literature.

To enable more rapid and sensitive measurements, we developed a digital EV screening technique (DEST) optimized for the analysis of scant surface and intravesicular EV proteins. The DEST method is a nearly single EV analytic technique with wide dynamic range and allows high throughput digital analysis of clinical samples (Figure 1). Here we show proof-of-principle of this approach, including rapid isolation that does not require lengthy ultracentrifugation and is thus clinically practical. After validation in cell lines and patient-derived xenograft (PDX) models, we applied these technical innovations to a discovery cohort of 86 patients and a validation cohort of 47 patients.

Methods

Specimen Acquisition

This study was approved by the Massachusetts General Hospital Institutional Review Board. Written informed consent was obtained from study participants. All specimens were collected from patients referred to Massachusetts General Hospital for surgical management. Participants were enrolled into a clinical discovery cohort or a validation cohort. The discovery cohort included healthy controls and patients with HG- or LG-IPMNs. The validation cohort comprised patients with IPMNs diagnosed on imaging. All of the patients in the validation cohort were monitored for at least 1 year, during which time unresected pancreatic lesions were serially surveilled according to established clinical criteria, including repeat imaging.[7,8] Cohort demographics and imaging features were recorded.

Clinical Sample Preparation

Blood collection was optimized for plasma EV analysis as described in Lobb et al,[11] and all samples were deidentified and analyzed in blinded fashion. Whole blood was collected in one 10-mL purple-top EDTA tube and was inverted 10 times to mix. Whole blood was stored upright at 4°C and processed within 1 hour of collection. To process blood for plasma isolation, the tube was centrifuged for 10 minutes at 400*g* (4°C). The plasma layer was collected in a 15-mL tube using a pipette to avoid disturbing the buffy coat. Plasma was then centrifuged for 10 minutes at 1100*g* (4°C), aliquoted into 10-mL aliquots, and stored at −80°C.

Extracellular Vesicle Isolation From Plasma

Optimized plasma EV isolation was done according to Lobb et al.[11] Briefly, plasma was thawed on ice, and 500 μL was centrifuged at 10,000*g* for 20 minutes at 4°C. A qEV original size exclusion column (SP1; Izon Science, Medford, MA) was equilibrated to room temperature and then flushed with 10 mL of 0.22-μm filtered phosphate-buffered saline (PBS). The plasma supernatant was loaded onto the column, and 0.5-mL fractions were immediately collected. Fractions 0 to 6 (dead volume) were discarded, and fractions 7 to 9 were collected (1.5 mL). Combined fractions 7 to 9 were concentrated using an Amicon 10K (15 mL; Millipore, Burlington, MA) and centrifuging at 3100*g* for 15 minutes. Total EV protein was measured using the Qubit protein assay (Q33211, Thermo Fisher

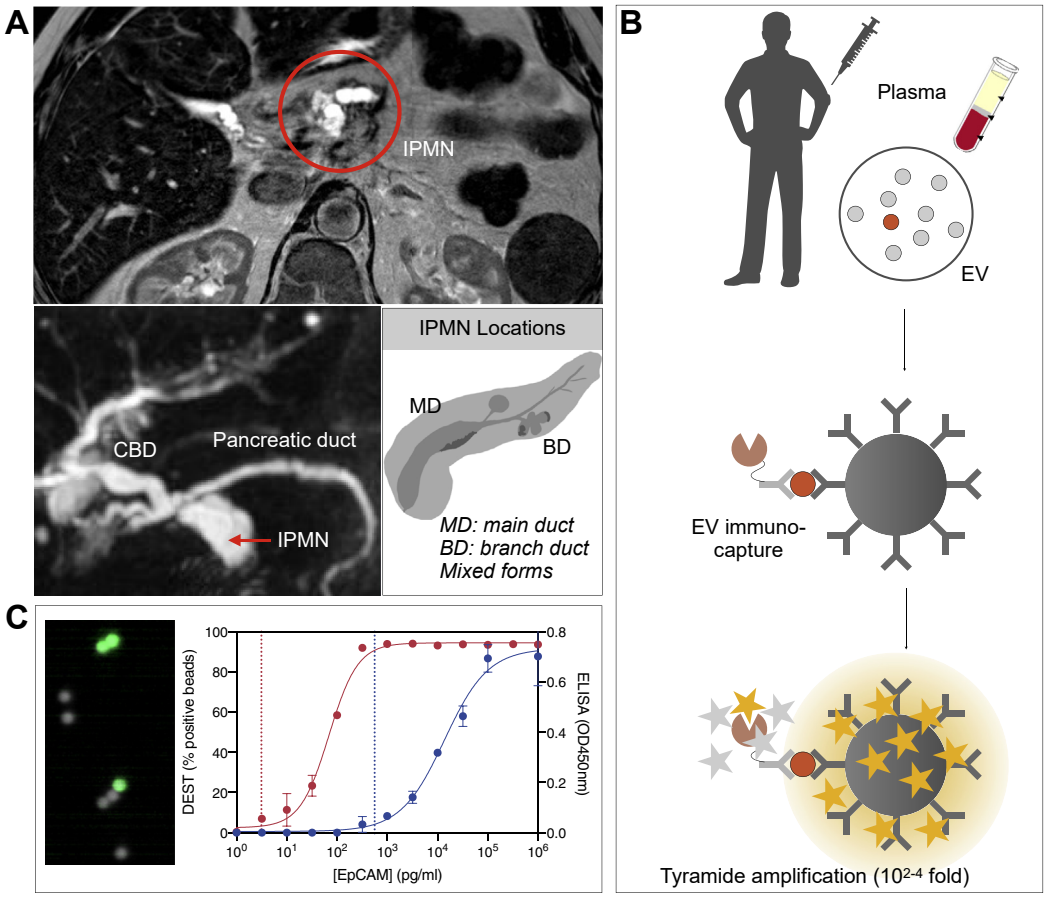

Figure 1. EV analysis for IPMN characterization. (*A*) IPMNs are often incidentally detected by abdominal imaging. Repeat MRI is used to monitor these T2-hyperintense lesions. Imaging alone has limited accuracy in separating benign from premalignant lesions that require resection. (*B*) Schematic diagram of the DEST assay. EVs are first captured on micron-sized beads via specific antibodies (see Supplementary Table 3), and their presence is then detected via complementary antibodies, followed by a tyramide signal amplification step. The presence of individual or multiple EVs on a bead renders the entire bead as fluorescent. (*C*) Analysis is done in high throughput by counting the number of fluorescent beads. Overall, the method is 3 to 4 orders of magnitude more sensitive than ELISA and uniquely suited to analyze rare EV subpopulations. The *dashed lines* represent the limit of detection for 1617 PDAC PDX EVs in the DEST (~100 EVs; *left dashed line*) or ELISA (~10^5 EVs; *right dashed line*) assay.

Scientific, Waltham, MA). Final experiments tailored for a clinical workflow used immunopurification inherent to the DEST assay to isolate EV proteins from unpurified plasma (see below). To reduce background in the DEST assay from plasma, we used various blocking buffers (2% bovine serum albumin, UltraBlock, and human anti-mouse antibody blocker; see DEST assay methods below).

Plasma Preparation

Unpurified plasma was lysed in radioimmunoprecipitation assay lysis buffer for use in the DEST assay to lyse EVs for intravesicular and extravesicular analysis. Plasma was thawed at 4°C and then lysed in 1X radioimmunoprecipitation assay buffer (9806S, 6X stock; Cell Signaling Technology, Danvers, MA) for 15 minutes on ice. Lysed plasma was aliquoted and stored at −80°C until use.

Extracellular Vesicle Isolation From Cell Culture

Cell-derived EVs were initially isolated by ultracentrifugation as the gold standard for validating both the Izon and direct method (Supplementary Figure 1). Cells were grown for 48 to 72 hours in normal growth medium supplemented with 5% exosome-depleted fetal bovine serum (A2720801, Thermo). Conditioned media were collected and centrifuged at 300*g* for 10 minutes to remove dead cells and debris, followed by filtration through a 0.22-μm cellulose acetate vacuum filter (430767; Corning, Corning, NY). Media were then aliquoted to ultracentrifuge tubes (344058; Beckman Coulter, Fullerton, CA) and centrifuged at 100,000*g* for 70 minutes to pellet EVs. Media were removed, and EV pellets were combined in a single ultracentrifuge tube in PBS, which was then centrifuged again at 100,000*g* for 70 minutes. The final EV pellet was resuspended at a volume of ~100 μL in PBS and stored at −80°C until use.

Digital Extracellular Vesicle Screening Technique Assay

Experimental steps, including incubation times and concentrations, are outlined in Supplementary Table 1. Reagents needed for the assay are listed in Supplementary Table 2, while antibody pairs, conditions, and controls are listed in

Supplementary Tables 3 and 4. Purified protein positive controls were used for thrombospondin-1 (TSP1; 3074-TH-050; R&D Systems, Minneapolis, MN), thrombospondin-2 (TSP2; 1635-T2-050; R&D), glypican 1 (GPC1; 4519-GP-050; R&D), wingless-type MMTV integration site family member 2 (WNT-2; 2104322; MyBioSource, San Diego, CA), S100 calcium-binding protein A4 (S100A4; 2089230, MyBioSource), and prostate stem cell antigen antibody (PSCA; 30R-3214; Fitzgerald, Acton, MA). Bead readout was done using a CytoFLEX flow cytometer (Beckman Coulter) with the following settings: forward scatter, 201V; side scatter, 90V; PB450 (BV421 detection), 40V. A gate was drawn around single beads, and 10,000 events were recorded for each sample and marker combination. Data were analyzed using FlowJo 10.6.1 software (BD Biosciences, San Jose, CA).

Briefly, pooled normal human plasma was used as a background control for the assay. A gate was drawn using the bisector tool to delineate positive from negative beads. All data are reported as percentage of positive beads of 10,000 total beads measured and are the average of duplicate measurements. Error is represented as the standard error of the mean. False positives were identified using human anti-mouse antibody blocker (Abcam, Cambridge, MA) during the plasma incubation step for mouse antibody pairs (mucin 1, cell surface associated [MUC1], mucin 5AC, oligomeric mucus/gel-forming [MUC5AC]) or isotype control beads (all other antibody pairs).

Statistics

Biomarkers and imaging comparison groups were categorized as (1) LG- vs noninvasive HG-IPMN, (2) LG vs inv/HG, or (3) LG- vs HG-IPMNs. For the discovery cohort, a Mann-Whitney test was used to compare individual biomarker levels between IPMN groups. Subsequently, classifiers were built on individual biomarkers using the continuous values and with the following combinations: (1) pancreatic ductal adenocarcinoma (PDAC)^{EV} signature (MUC1 + GPC1 + epidermal growth factor receptor [EGFR] + epithelial cell adhesion molecule [EpCAM] + WNT-2), and (2) DEST MUC5AC + imaging values. Diagnostic performance of these classifiers was assessed by a receiver operating characteristic (ROC) curve, 95% confidence intervals, F1 scores, and χ^2 tests for discovery cohorts. The optimum cutoff value(s) for each classifier was calculated based on Youden's index, and the final value was manually selected when multiple optimal cutoffs were found. The 95% confidence intervals were estimated by bootstrapping (n = 5000 bootstrapped samples). For validation, only MUC5AC, imaging, and MUC5AC + imaging were included. Logistic regression equations derived in the discovery cohort were applied to assess diagnostic performance. Classifier performance metrics were calculated the same way as described for the discovery cohort. Specificity, sensitivity, and positive predictive values reported for the validation cohorts were based on the optimal thresholds chosen from the discovery cohort. Main analyses were performed using the pROC package in R 3.6.2 software (R Foundation for Statistical Computing, Vienna, Austria).[12]

Results

Clinical and Pathologic Features

The study enrolled 133 participants. The discovery cohort (n = 86) comprised healthy controls (n =10), age-matched healthy controls (benign) undergoing abdominal surgery but without evidence of any pancreatic lesion (n = 14), patients with IPMNs harboring LG dysplasia (n = 40), and patients (n = 22) with HG-IPMN (11 with HG dysplasia and 11 with inv/HG). The validation cohort was divided into patients with LG dysplasia, confirmed at surgery or on the basis of imaging findings and temporal stability (n = 35) or HG dysplasia, confirmed at resection (n = 12). In the validation cohort, 19 patients underwent surgical resection, which yielded 9 lesions with HG dysplasia and 3 lesions with invasive IPMN. The remaining 7 patients were LG-IPMNs. Clinical and imaging features for each cohort are summarized in Table 1.

Digital Extracellular Vesicle Screening Analysis Has Nearly Single Extracellular Vesicle Sensitivity

Analysis of scant circulating EVs produced by small tumors requires new ultrasensitive diagnostic assays because bulk detection methods are unlikely to detect human tumors <1 cm^3. Although some single EV analytic methods have been described as research tools,[13–15] they often have limited clinical applications because the methods are too labor intensive, costly, or have limited multiplexing capability. To enable detection of HG-IPMN and early invasive pancreatic cancers, we thus set out to first develop and optimize a bead-based digital enzyme-linked immunosorbent assay (ELISA) assay adopted for EV analysis.

The DEST method uses magnetic beads coated with capture antibodies, biotinylated detection antibody, and intact or lysed EVs to capture surface or intravesicular proteins, respectively (Figure 1*B*). To ensure the most sensitive readout, the DEST assay includes a tyramide signal amplification step that catalyzes the addition of biotin groups on or near horseradish peroxidase from tyramide-biotin radicals.[16] Brilliant violet 421 conjugated to streptavidin labels all free biotin molecules for ultrabright readout of micron-sized beads by cytometry. As shown in Figure 1*C*, bead readout is digital with a bead either being fluorescent or not. To compare the sensitivity of the DEST assay to traditional ELISA, we compared EpCAM analysis in EVs from a low-passage patient-derived PDAC cell line (#1617). Traditional ELISA has a limit of detection of ~1 million EVs, whereas DEST has a limit of detection of ~100 EVs based on EpCAM analysis (Figure 1*C*). This 10,000-fold increase in sensitivity may enable detection of ultrarare EVs and low-abundance proteins. Additional benefits of the DEST method include analysis times of <2 hours from start to finish, the ability to process hundreds of samples per day, and the relatively low cost.

Choice of Extracellular Vesicle Biomarkers and Correlation to Cellular Signatures

To determine which EV biomarkers could be useful in differentiating LG- and HG-IPMN, we first surveyed the literature on biomarkers.[17–41] We identified 22 putative biomarkers, some of which had been used to analyze pancreatic cyst fluid obtained by interventional endoscopy.[18,19,22,24,25,29,35] Circulating TSP2 and MUC5AC levels have been tested in pancreatic cancer, but not for the ability to distinguish LG- and HG-IPMN.[21,28] The chosen 22 biomarkers for which antibody pairs were commercially available include MUC1, mucin 2 (MUC2), mucin 4 (MUC4),

Table 1. Summary of Patient Cohorts and Clinical Findings

	Patients	Discovery cohort							Validation cohort			
						HG-IPMN					HG-IPMN	
Characteristic	All	All	Control	Benign	LG	Inv	Noninv	Comb	All	LG	Inv	Noninv
Total cases	133	86	10	14	40	11	11	22	47	35	3	9
Age, *y*												
Median	71	70	33	54	72	79	71	73	74	71	76	76
IQR	63–77	59–76	27–47	40–62	68–78	67–84	68–74	68–80	67–77	65–76	73–83	75–78
Sex, No.												
Male	55	38	6	7	15	5	5	10	17	16	0	1
Female	78	48	4	7	25	6	6	12	30	19	3	8
Clinical, No.												
Symptoms	43	38	NA	12	15	6	5	11	5	1	1	3
Weight loss	23	17	NA	2	9	3	3	6	6	1	3	2
Pain	31	28	NA	11	12	2	3	5	3	1	0	2
Jaundice	2	2	NA	0	0	2	0	2	0	0	0	0
Laboratory values, No.												
CA19-9 >37 U/mL	13	11	NA	3	4	3	1	4	2	0	2	0
Imaging, No.												
Duct >10 mm	12	9	NA	0	2	3	4	7	3	0	2	1
Duct 5-9 mm	26	17	NA	1	7	3	6	9	9	2	1	6
Cyst >3 cm	43	32	NA	6	18	2	6	8	11	6	2	3
Thickened wall	7	4	NA	1	1	0	2	2	3	1	1	1
Enhancing nodule	13	8	NA	2	1	3	2	5	5	0	2	3
Pancreatitis	21	20	NA	9	7	1	3	4	1	0	0	1
Adenopathy	0	0	NA	0	0	0	0	0	0	0	0	0
Surgery, No.												
None	44	16	10	0	15	1	0	1	28	28	0	0
Whipple	32	22	NA	4	12	6	10	16	10	2	2	6
Pancreatectomy												
Distal	22	13	NA	4	8	1	1	2	9	5	1	3
Middle	6	6	NA	2	4	0	0	0	0	0	0	0
Total	2	2	NA	0	0	2	0	2	0	0	0	0
Puestow	2	2	NA	2	0	0	0	0	0	0	0	0
Other	4	4	NA	2	1	1	0	1	0	0	0	0

NOTE. Control: healthy control patients; benign: age-matched control patients undergoing abdominal surgery but without evidence for any pancreatic lesions. Patients with HG-IPMN are divided into invasive (Inv) and noninvasive (Noninv) forms. Comb, combined; IQR, Interquartile range; NA, not applicable.

MUC5AC, mucin 6 (MUC6), Das-1, stathmin 1 (STMN1), TSP1, TSP2, EGFR, EpCAM, GPC1, WNT-2, EPH receptor A2 (EphA2), S100A4, PSCA, mucin 13 (MUC13), zinc finger E-box-binding homeobox 1 (ZEB1), plectin (PLEC1), hook microtubule tethering protein 1 (HOOK1), protein tyrosine phosphatase non-receptor type 6 (PTPN6), and fibrillin-1 (FBN1). For each of these targets, we had to identify reliable antibody pairs for protein capture and detection to establish the assay. We tested most commercially available antibodies to find suitable pairs, but not all of them worked well. This may be due to steric hindrance, low affinity, or the polyclonality of some commercial products. Supplementary Figure 2 and Supplementary Table 3 summarize the 16 antibody pairs that ultimately proved reliable, and Supplementary Table 5 lists pairs unsuitable for DEST.

For each antibody pair, we next determined positivity (against control-matched immunoglobulin G) and thus detection sensitivity. To enable clinical measurements, we optimized the method so that only 1 to 10 μL of plasma was necessary per measurement. To minimize the loss of potential very rare IPMN EVs, we also compared different EV purification steps (Supplementary Figure 1). We found that many traditional methods, such as ultracentrifugation and Izon column purification, resulted in considerable loss or shift of EV subpopulations and also required large amounts of plasma. We thus settled on simple direct EV processing from unpurified plasma, because the DEST assay includes an immunocapture "purification" as the first step (Supplementary Figure 1). Combined, this workflow is suited for the clinical setting where sample

volume is limited and throughput is an important consideration.

Thus, established and validated DEST assays were next tested in whole-cell lysates and EVs of IPMN and PDAC PDX models. As shown in Supplementary Figure 2, the DEST signal from EVs generally correlated with the whole-cell signal for a given biomarker (or its absence). We were particularly interested in the signals from 2 inv/HG-IPMN PDX cell lines, #1966 and #1505, because these may inform on HG-IPMN patient samples. In the IPMN PDX EVs, the most abundant markers were MUC5AC and MUC6.

Analysis of Extracellular Vesicle Biomarkers in Clinical Intraductal Papillary Mucinous Neoplasms Discovery Cohort

We next measured the 16 validated EV proteins in plasma samples collected from a clinical patient cohort (n = 86, Table 1) that included healthy controls (n = 10), age-matched benign controls (n = 14), LG-IPMN (n = 40) and HG-IPMN (n = 22). These groups were chosen not based on imaging findings but rather to reflect the expected spectrum of EV profiles from clearly negative (healthy) to positive (HG-IPMN). Figure 2 and Figure 3*A* summarize the biomarker expression in the 4 patient categories for all 16 biomarkers. For most of the markers tested, we did not see a significant difference between LG-IPMN and HG-IPMN (Figure 2, blue vs red; Mann-Whitney test, $P < .05$; Table 2, Supplementary Figure 3 ROC curve analysis).

This negative result was of interest because we had expected to be able to differentiate mucinous neoplasm subtypes by pan MUC-EV analysis that had first been proven to be useful in cyst fluid analysis.[25,36] We found that only MUC5AC showed significantly higher levels in HG lesions (Table 2). MUC5AC is a high-molecular-weight secreted glycoprotein that has been associated with certain pulmonary diseases and malignant transformation in tissue sections of IPMN.[42] However, pancreatic MUC5AC had not been shown to circulate in EV. The HG-IPMN group had higher MUC5AC levels, but interestingly, there was a bimodal distribution (Table 1).

Further analysis of pathology data showed that of the 11 patients with invasive carcinoma arising in HG-IPMN, referred to hereafter as inv/HG, 9 had high MUC5AC expression in plasma EV, and of the 11 patients with HG dysplasia alone, only 1 had high MUC5AC expression (Figure 3*B*, Supplementary Figure 4). This resulted in a specificity of 100%, a sensitivity of 82%, with an overall diagnostic accuracy of 96% for differentiating invasive IPMN from LG-IPMN by MUC5AC measurements alone (Table 2). This suggests that MUC5AC in circulating EVs may predict invasiveness of HG-IPMN and identify a patient cohort requiring surgical intervention. Future studies are required to determine the specificity in the presence of other comorbidities.

Two other markers showed small differences between cohorts. GPC1 was slightly lower in HG-IPMN compared with LG-IPMN (Figure 2, Supplementary Figure 4). This was an interesting inverse finding, because GPC1 has been associated with malignancy in some studies[43] but not in others.[44] However, previous pathologic studies of IPMN tissue also suggest that GPC1 is slightly higher in LG-IPMN vs HG-IPMN (56% positive rate vs 46%, respectively),[45] consistent with our findings here.

Another marker that was slightly higher in HG-IPMN was TSP1, although the overall TSP1 levels in HG-IPMN were very low and near background with considerable overlap to be clinically useful (Figure 2, Supplementary Figure 4). TSP1 by itself only had moderate sensitivity (68%) and specificity (93%) for diagnosing HG-IPMN (Table 2, Supplementary Figure 3). TSP1 is a large adhesive glycoprotein involved in cell-to-cell and cell-to-matrix interactions. Previous studies had suggested that circulating TSP1 expression decreases in PDAC compared with normal and benign pancreatic controls,[46,47] whereas another study suggested stromal TSP1 tissue expression was an indicator of IPMN invasiveness.[26]

Surprisingly, none of the other markers tested here showed a significant difference in EVs between LG-IPMN and HG-IPMN (Figures 2 and 3, Table 2). This included Das-1, a protein shown in pancreatic cyst fluid and histologic sections to differentiate between HG- and LG-IPMN.[25] The bubble plot in Figure 3*C* compares 4 different statistical parameters (fold-change in biomarker signal, -log *P* value, area under the curve [AUC], and F1 score), demonstrating that MUC5AC is superior to the other biomarkers tested in identifying inv/HG-IPMN from indolent LG-IPMN.

Analysis of Extracellular Vesicle Biomarkers in Clinical Intraductal Papillary Mucinous Neoplasms Validation Cohort

We next remeasured the 16 validated EV proteins in plasma samples collected in the validation cohort (Supplementary Figure 5). Our results show that the 3 patients with inv/HG-IPMN had high MUC5AC expression in plasma EVs (Supplementary Table 6). None of the patients in the LG dysplasia cohort had high MUC5AC expression. MUC5AC EV levels were highest in invasive HG lesions and low in LG lesions. In the combined cohorts of HG and invasive lesions, the specificity of this biomarker for identifying invasive disease was 97% to 100%, the sensitivity was 33% to 50%, and the AUC was 0.648 to 0.727 (Table 2, Figure 4*B*, Supplementary Figure 3). The values for differentiating LG and HG (noninvasive) lesions was specificity, 91% to 100%; sensitivity, 11% to 32%; and AUC, 0.545 to 0.648. Interestingly, neither GPC1 nor TSP1 expression showed a significant difference between LG-IPMN and HG-IPMN in the validation cohort.

Integrating Extracellular Vesicle Testing With Imaging Improves Intraductal Papillary Mucinous Neoplasms Analysis

Magnetic resonance cholangiopancreatography is an established and noninvasive method for the initial evaluation and surveillance of IPMNs[48] but lacks specificity for the reliable distinction of LG- from HG-IPMNs. IPMNs are

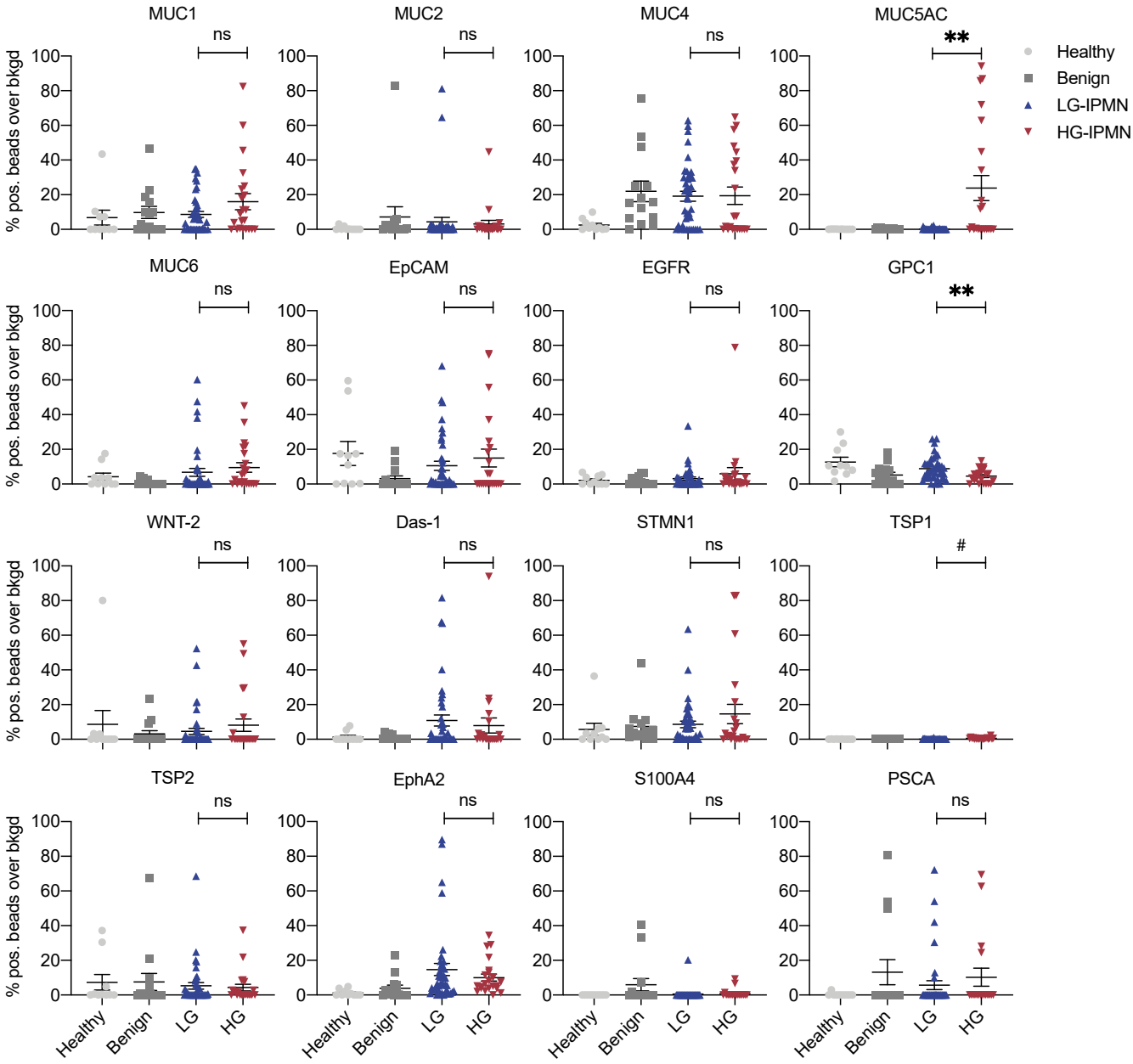

Figure 2. Analysis of 16 prototypical biomarkers in EVs from different patient groups. Each data point represents an EV sample from a single patient. Data shown are from healthy controls (n = 10); benign (age-matched control patients undergoing abdominal surgery but without evidence for any pancreatic lesions; n = 14); LG-IPMN (n = 40 patients), and HG-IPMN (n = 22 patients). See Table 1 for cohort demographics. Differences between HG-IPMN and LG-IPMN: $^{**}P < .01$, ns = not statistically significant ($P > .05$). #TSP1 is statistically significant but the extremely low signal over background makes the results clinically unreliable. The *error bars* show the standard error of the mean.

morphologically divided into main-duct, branch-duct, or mixed-type. Resection is indicated upon diagnosis of main-duct and mixed-type IPMNs, defined as main pancreatic duct diameter >10 mm, due to their high malignant potential. However, the management of branch-duct IPMNs is more nuanced because their incidence of malignancy is significantly lower. Surgical resection is indicated in the presence of high-risk features including jaundice, an enhancing nodule >5 mm, or dilated pancreatic duct >10 mm. When worrisome features are identified, such as a cyst diameter ≥3 cm or >5 mm growth over 2 years, thickened cyst walls, enhancing septations or nodules <5 mm, main duct diameter 5 to 9 mm with pancreatic atrophy or lymphadenopathy, further evaluation with endoscopic ultrasound is then required.[5] Patients who do not meet requirements for surgical resection undergo imaging surveillance at varying intervals. The performance profile of these diagnostic imaging features reported elsewhere was similar in our cohort, with a low specificity at ROC curve analysis shown in Figure 4*A*, Table 2, and Supplementary Table 5. Given the modest specificity of

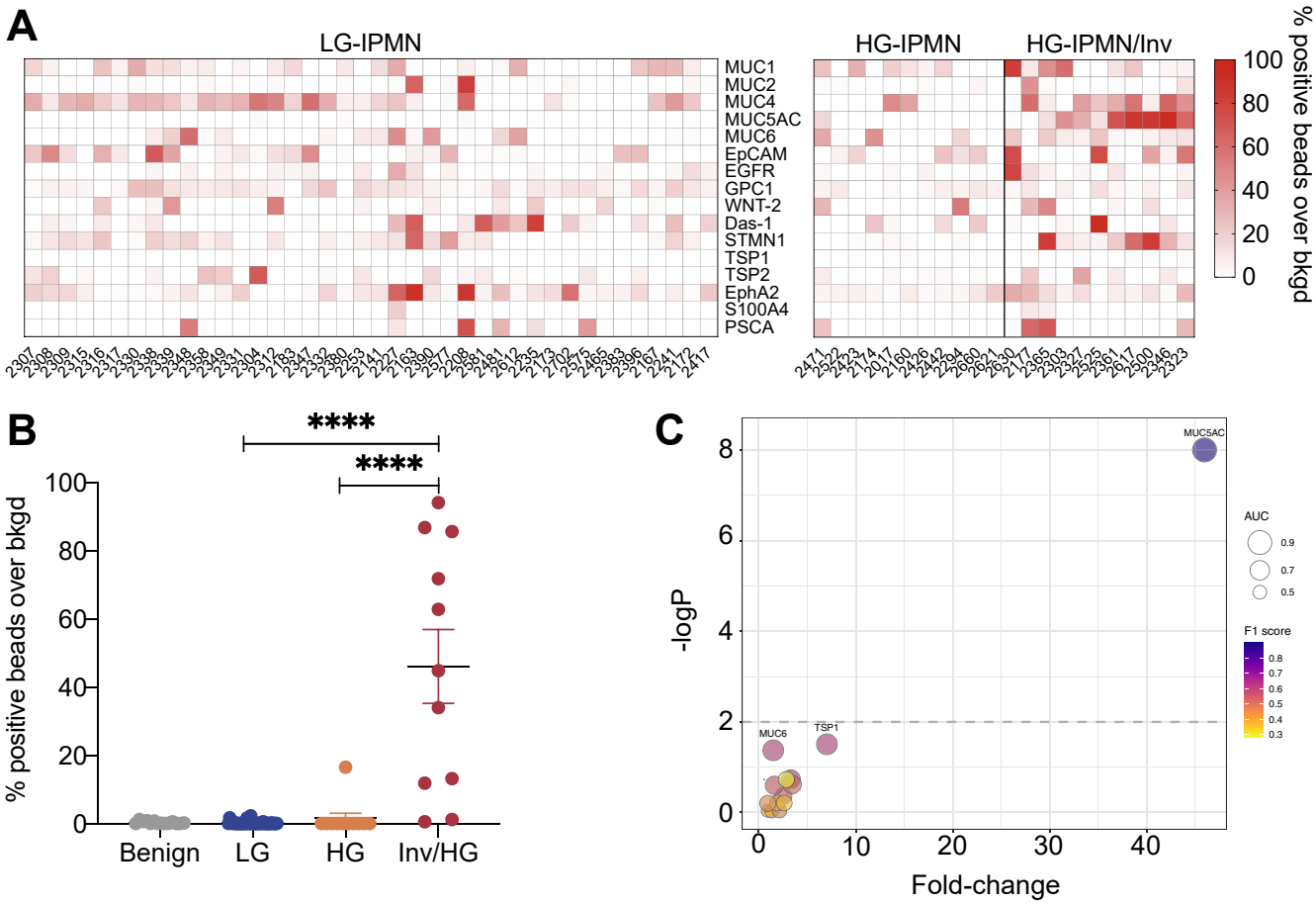

Figure 3. Discovery cohort analysis. (*A*) EV biomarker analysis across all patients with IPMN. Each column refers to a single patient. Patients are grouped into LG-IPMN, HG-IPMN, and inv/HG IPMN determined by pathology. Notable differences between the groups can be seen for MUC5AC. (*B*) Subgroup comparison of MUC5AC-positive EVs. Note the significantly higher levels in invasive HG-IPMN against noninvasive HG-IPMN or LG-IPMN. ****$P < .0001$ by Mann-Whitney, 2-tailed. The *error bars* described the standard error of the mean. (*C*) Bubble plot of each molecular EV biomarker tested. The graph summarizes the following descriptive statistics: fold-change over LG-IPMN (*x*-axis), -log *P* value by Mann-Whitney test (*y*-axis), and classifier metrics: AUC (bubble size), and F1 score (bubble color). Highly predictive EV biomarkers reside in the upper right hand corner. Only MUC5AC EV analysis stood out in the discovery cohort.

imaging, we asked whether combined analyses with EV testing would improve diagnostic performance.

Figure 4 summarizes the ROC curve of imaging alone and combined imaging and DEST analysis (MUC5AC EV), whereas Table 2 and Supplementary Table 6 provide additional metrics on accuracy for the different parameters. Our results indicate (1) HG-IPMN can be distinguished from LG-IPMN with high sensitivity and specificity when MUC5AC and imaging are combined (Figure 4*C* vs Figures 4*A* and *B*) and (2) MUC5AC alone identifies inv/HG-IPMN with high sensitivity and specificity (Figure 4*D*). If currently established tools for stratifying IPMN risk had been used in isolation to guide surgical intervention, including imaging features or high-risk stigmata, then 5 of 14 patients (36%) would not have proceeded to surgery. When MUC5AC was added, all patients would have been correctly identified (Supplementary Figure 6).

Overall, our results suggest that the likelihood of inv/HG-IPMN in the absence of elevated MUC5AC levels is low. Figure 5 summarizes this in a clinical example. A patient with an incidentally detected IPMN had been monitored with yearly MRI for more than a decade, showing a progressive increase in IPMN size. A clinical decision was made to resect the growing IPMN, but this led to perioperative complications requiring an extended hospital stay. Pathologic analysis confirmed a LG-IPMN without evidence for any invasive features. In this case, MUC5AC was not detectable in EVs, and therefore, this lesion would have been correctly classified as LG-IPMN through EV analysis.

Discussion

The prevalence of pancreatic cysts in the general population is unexpectedly high and increases in number and size with age.[10,49] As discussed, the increased detection of IPMNs at cross-sectional imaging warrants a burdensome program of surveillance that potentially places enormous constraints on modern health care systems. Furthermore,

Table 2. Extracellular Vesicle Biomarker Accuracy for the Diagnosis of Invasive and Noninvasive High-Grade Compared With Low Grade Intraductal Papillary Mucinous Neoplasms in the Discovery Cohort

	Invasive HG-IPMN			Noninvasive HG-IPMN			Combined HG-IPMN		
Biomarker(s)	Sensitivity	Specificity	Accuracy	Sensitivity	Specificity	Accuracy	Sensitivity	Specificity	Accuracy
MUC1	0.45 (0.09–0.91)	0.90 (0.43–1.00)	0.80 (0.51–0.90)	0.45 (0.00–1.00)	0.80 (0.00–1.00)	0.68 (0.55–0.77)	0.45 (0.09–0.82)	0.80 (0.45–1.00)	0.68 (0.55–0.77)
MUC2	0.73 (0.36–1.00)	0.55 (0.03–0.83)	0.59 (0.24–0.76)	0.73 (0.36–1.00)	0.53 (0.03–0.83)	0.58 (0.37–0.71)	0.32 (0.00–1.00)	0.83 (0.00–1.00)	0.65 (0.35–0.73)
MUC4	0.55 (0.00–1.00)	0.65 (0.00–1.00)	0.61 (0.22–0.78)	0.82 (0.55–1.00)	0.75 (0.63–0.88)	0.66 (0.53–0.77)	0.36 (0.09–0.59)	0.9 (0.78–1.00)	0.69 (0.61–0.79)
MUC5AC	0.82 (0.55–1.00)	1.00 (1.00–1.00)	0.96 (0.90–1.00)	0.09 (0.00–1.00)	1.00 (0.00–1.00)	0.81 (0.73–0.87)	0.45 (0.27–0.68)	1.00 (1.00–1.00)	0.81 (0.74–0.89)
MUC6	0.91 (0.64–1.00)	0.70 (0.53–0.85)	0.75 (0.61–0.86)	0.27 (0.00–1.00)	0.90 (0.00–1.00)	0.68 (0.56–0.79)	0.59 (0.27–0.82)	0.73 (0.55–0.95)	0.68 (0.56–0.79)
EpCAM	0.64 (0.00–1.00)	0.60 (0.00–1.00)	0.59 (0.22–0.78)	1.00 (0.55–1.00)	0.28 (0.10–0.73)	0.58 (0.35–0.69)	0.59 (0.00–1.00)	0.6 (0.00–1.00)	0.58 (0.35–0.69)
EGFR	0.82 (0.27–1.00)	0.60 (0.40–1.00)	0.65 (0.51–0.86)	0.55 (0.00–1.00)	0.55 (0.00–1.00)	0.61 (0.50–0.73)	0.64 (0.05–0.86)	0.6 (0.38–1.00)	0.61 (0.50–0.71)
GPC1	0.73 (0.36–1.00)	0.70 (0.23–0.95)	0.71 (0.39–0.86)	0.91 (0.45–1.00)	0.58 (0.30–0.93)	0.68 (0.53–0.81)	0.82 (0.41–1.00)	0.60 (0.30–0.95)	0.68 (0.53–0.81)
WNT-2	0.36 (0.00–1.00)	0.90 (0.00–1.00)	0.78 (0.22–0.84)	0.18 (0.00–1.00)	0.98 (0.00–1.00)	0.68–0.61–0.76)	0.23 (0.05–0.5)	0.95 (0.75–1.00)	0.68 (0.61–0.76)
Das-1	0.91 (0.64–1.00)	0.43 (0.18–0.60)	0.51 (0.33–0.67)	1.00 (0.73–1.00)	0.30 (0.08–0.58)	0.55 (0.42–0.660	0.82 (0.64–1.00)	0.40 (0.10–0.60)	0.55 (0.40–0.66)
STMN1	0.55 (0.00–1.00)	0.55 (0.00–1.00)	0.55 (0.22–0.78)	1.00 (0.91–1.00)	0.58 (0.40–0.75)	0.60 (0.39–0.71)	0.64 (0.23–1.00)	0.58 (0.00–0.90)	0.60 (0.35–0.71)
TSP1	0.64 (0.27–0.91)	0.88 (0.63–1.00)	0.82 (0.65–0.92)	0.82 (0.55–1.00)	0.95 (0.85–1.00)	0.84 (0.73–0.92)	0.68 (0.45–0.91)	0.93 (0.73–1.00)	0.82 (0.73–0.90)
TSP2	0.36 (0.00–0.91)	0.88 (0.50–1.00)	0.76 (0.53–0.84)	0.55 (0.00–1.00)	0.63 (0.00–1.00)	0.63 (0.35–071)	0.45 (0.00–1.00)	0.70 (0.00–1.00)	0.63 (0.35–071)
EphA2	0.73 (0.18–1.00)	0.65 (0.22–0.95)	0.65 (0.37–0.84)	1.00 (0.73–1.00)	0.30 (0.08–0.55)	0.53 (0.42–0.69)	0.86 (0.18–1.00)	0.35 (0.13–0.95)	0.53 (0.42–0.69)
S100A4	0.18 (0.00–1.00)	0.98 (0.00–1.00)	0.80 (0.22–0.86)	0.09 (0.00–1.00)	0.98 (0.00–1.00)	0.68 (0.35–0.74)	0.14 (0.00–1.00)	0.98 (0.00–1.00)	0.68 (0.35–0.74)
PSCA	0.27 (0.00–1.00)	0.95 (0.00–1.00)	0.80 (0.22–0.86)	0.18 (0.00–1.00)	0.93 (0.00–1.00)	0.66 (0.35–0.73)	0.18 (0.00–1.00)	0.95 (0.00–1.00)	0.66 (0.35–0.73)
PDAC^{EV}	0.70 (0.55–0.88)	1.00 (0.82–1.00)	0.76 (0.65–0.88)	0.72 (0.32–0.98)	0.82 (0.45–1.00)	0.75 (0.47–0.90)	0.68 (0.40–0.85)	0.86 (0.68–1.00)	0.74 (0.60–0.84)
Imaging alone	0.27 (0.1–0.57)	0.88 (0.74–0.94)	0.65 (0.53–0.75)	0.55 (0.28–0.79)	0.88 (0.74–0.95)	0.77 (0.65–0.87)	0.41 (0.23–0.64)	0.88 (0.78–0.98)	0.71 (0.61–0.81)
DEST+imaging	0.95 (0.64–1.00)	1.00 (0.71–1.00)	0.93 (0.70–1.00)	1.00 (1.00–1.00)	1.00 (1.00–1.00)	1.00 (1.00–1.00)	0.73 (0.45–0.91)	0.88 (0.78–1.00)	0.82 (0.74–0.92)

NOTE. All numbers for sensitivity, specificity, and accuracy are in fractions, with the 95% confidence interval in parenthesis.

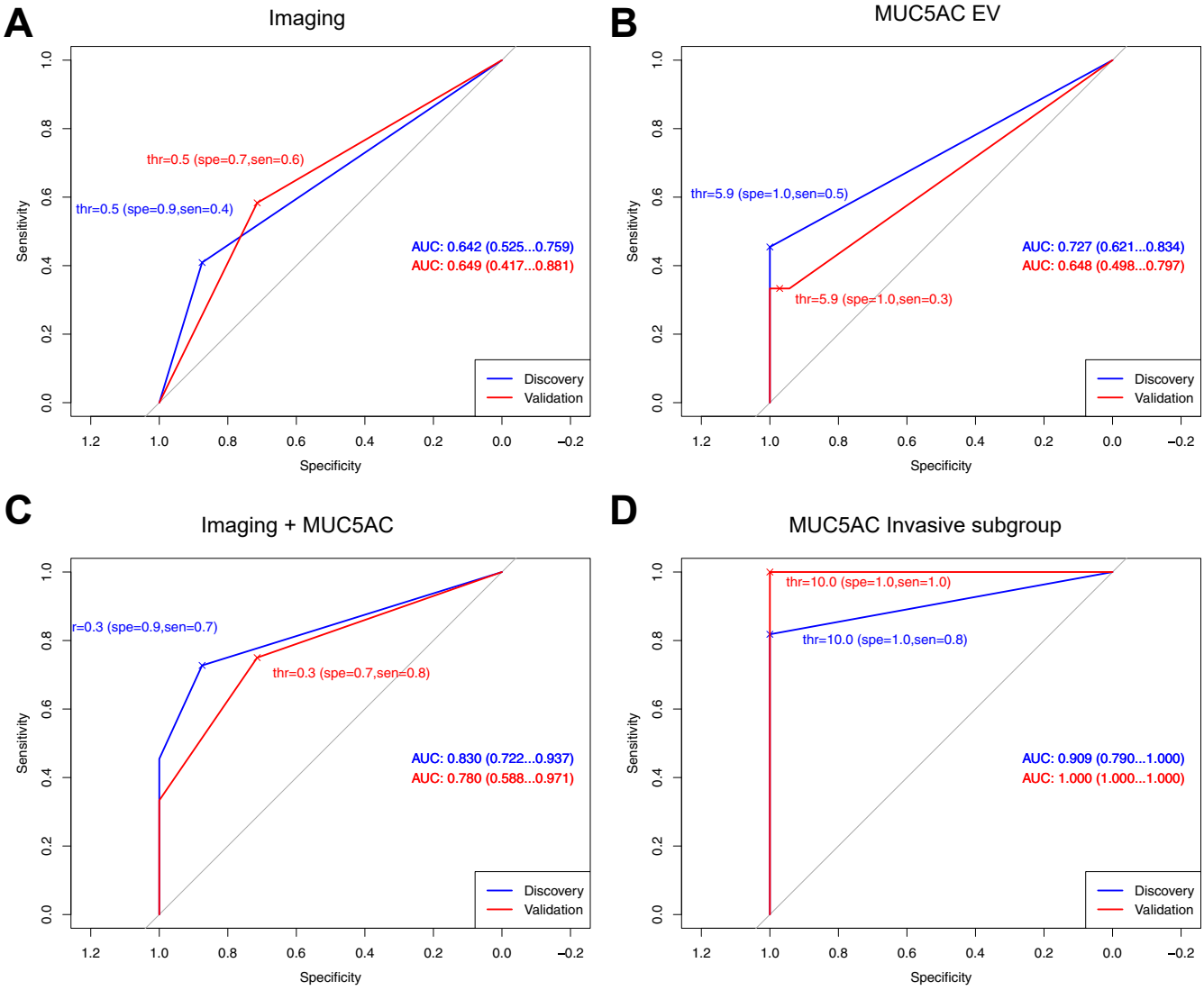

Figure 4. ROC curve analyses of imaging and MUC5AC-EV in discovery and validation cohorts. (*A*) ROC curve analysis for differentiating HG-IPMN from LG-IPMN by imaging alone. AUCs (95% confidence interval) are shown. Thr: threshold; spe: specificity; sen: sensitivity. (*B*) AUC for MUC5AC EV. (*C*) Combined imaging and MUC5AC analysis shows an improved AUC in both cohorts. (*D*) MUC5AC EV analysis for inv/HG-IPMN (without imaging combination). Note the high AUC in this important subgroup. Optimal cutoff thresholds were chosen from discovery and applied to the validation cohort analyses to display specificity and sensitivity at the chosen thresholds.

the possible requirement for ancillary invasive testing, including endoscopic ultrasound or surgical resection, are often undertaken with an appreciation of the poor diagnostic performance of imaging features alone to distinguish LG indolent subtypes from HG dysplastic lesions. While pancreatic cyst fluid can be analyzed, it requires sampling by endoscopic ultrasound, but this is invasive and costly, and therefore not practical as a multiple repeated test.[25] Blood-based tests are thus of high medical interest to manage these potentially large patient populations in a cost-effective manner, and more accurate markers of high-grade dysplasia or early invasive carcinoma could support potentially curative resection on the one hand and obviate the need for unnecessary resection on the other. Ideally, one would like to have blood biomarkers that could be serially analyzed.

To date, most biomarkers have focused on mutational aberrations,[8,36,50] protein,[33,51,52] and EV analysis. Aberrant protein/EV markers indicative of malignancy often include panels of proteins such as carbohydrate antigen (CA) 125, EGFR, MUC1, GPC1, WNT2, EpCAM, mutant KRAS,[37,53,54] as well as CA19-9 (and related glycans/isoforms).[55,56] CA 19-9 is the only United States Food and Drug Administration-approved biomarker for PDAC; however, its utility in identifying HG-IPMN is poor, as shown in a recent study of >500 IPMN patients by Ciprani et al.[57] Similar results are described here for the discovery cohort (Supplementary Figure 7). CA 19-9 is moderately useful in identifying invasive cancer with a sensitivity of 84.5%, but the specificity is only 40.8%.[57] Conversely, a much larger panel of proteins have been associated with PDAC in smaller studies, and their utility remains to be validated in larger trials (eg, CD73, TIMP1, LRG1, MSLN,

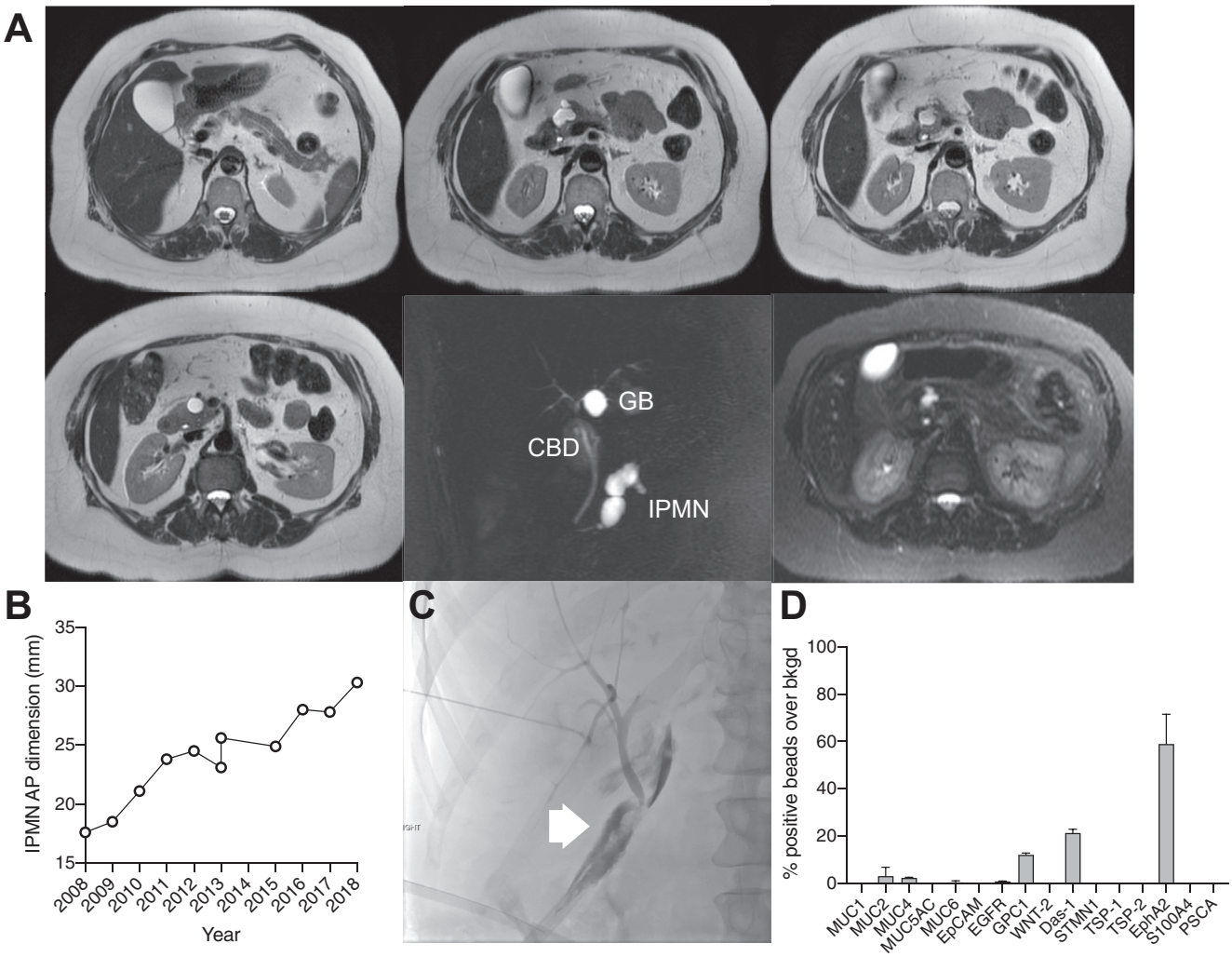

Figure 5. Enlarging IPMN concerning for HG dysplasia in a 57-year-old patient. (*A*) A predominantly branch-duct IPMN was monitored annually with MRI more than a decade. CBD, common bile duct; GB, gallbladder. (*B*) During this time, the anteroposterior (AP) size of the IPMN increased. (*C*) The patient underwent a pancreaticoduodenectomy. The postoperative course was prolonged by a bile leak that was treated by percutaneous biliary drainage (*arrow*). The pathology results showed an LG-IPMN. (*D*) Note that the MUC5AC EV levels at the time of surgery were low, indicative of an LG lesion and suggesting that surgery and the complicated postoperative course could have been avoided by EV analysis. The *error bars* show the standard error of the mean.

EphA2, GNAS, RNF43).[52,58] Many of the published studies are retrospective, consisted of small cohorts, relied on surgically resected specimens, and required cyst fluid rather that peripheral blood and analyzed mutations. In general, results have not been universally reproducible. Finally, most series do not differentiate between PDAC arising from IPMN (~25%) vs independently (~75%).

During several recent consensus meetings the guidelines for predicting invasive carcinoma and HG dysplasia, surveillance, and postoperative follow-up of IPMN have been revised.[5,6,59] Despite this, identifying which patients are at high risk of harboring or developing HG or invasive PDAC is challenging. Ideally, these patients should undergo resection, and as yet, the continued management and surveillance of those who do not undergo resection is controversial. More recently, nomograms have been developed to aid in the clinical decision making.[8,60]

Despite these recommendations and tools, differences remain in practice patterns around the world, and there is uncertainty on best approaches. What is very clear, however, is that (1) missed HG and early invasive PDAC will become unresectable if not operated on in a timely fashion, (2) long-term follow-up of LG-IPMN is expensive, burdensome, and often ambiguous, and (3) better diagnostics are urgently needed to improve clinical decision making, prevent unnecessary operations, and thus, advance the field.

Tumor-derived EVs and potentially host cell–derived EVs represent promising biomarkers in the analysis of pancreatic precursor lesions. Technologic advances have improved our ability to measure rare EV populations in plasma or cyst fluid, or both.[61] These advances are partly due to miniaturization of detection technology,[61] integrated sensor platforms capable of point-of-care testing in a clinical environment, digital sensing approaches,[62] and single-

vesicle analysis platforms,[13,15] among others. It is increasingly clear that EVs are secreted from cancer cells at higher rates than normal cells and can be identified in the blood of patients with pancreatic cancer.[53,63,64] The challenge, however, is to develop analytical methods with nearly single EV capabilities to detect rare tumor EVs from small lesions against a high background of normal host cell EVs. With such technologies in hand, we estimate that human cancers <1 mm^3 could be detectable.[65] Furthermore, any such assay has to be practical and high throughput so that it can be deployed clinically.

In the current study, we developed a digital ELISA approach for EV analysis (DEST) that allows high throughput measurements of clinical samples. We show that high MUC5AC measurement in EVs has a high predictive power to detect invasive HG-IPMN but was not elevated in LG-IPMN (AUC, 0.9; adjusted $P = 4.4 \times 10^{-10}$ for discovery cohort; AUC, 1.0; adjusted $P = 5.63 \times 10^{-8}$ for validation cohort). This measurement was markedly better than imaging alone (AUC, 0.6; adjusted $P = .23$ for discovery cohort; AUC, 0.5; adjusted $P = .28$ for validation cohort) and has a high predictive power.

Conclusion

We show that a simple blood-based test can effectively identify IPMNs with invasive carcinoma. EV profiling has the potential to improve triage of patients with worrisome lesions identified by imaging or endoscopic ultrasound and therefore avoid unnecessary operations but could also eventually simplify the care of all patients with pancreatic cysts that are currently managed with recurrent imaging. If larger prospective studies show that serial EV profiling can identify when an IPMN has become malignant, this test could have a major impact in the detection and care of pancreatic cancer, particularly if the addition of new EV biomarkers emerging from proteomic studies permit for the identification of HG dysplasia.[66–68]

Supplementary Material

Note: To access the supplementary material accompanying this article, visit the online version of *Gastroenterology* at www.gastrojournal.org, and at https://doi.org/10.1053/j.gastro.2020.11.046.

References

1. Gaujoux S, Brennan MF, Gonen M, et al. Cystic lesions of the pancreas: changes in the presentation and management of 1,424 patients at a single institution over a 15-year time period. J Am Coll Surg 2011;212:590–600; discussion: 600.
2. Maitra A, Fukushima N, Takaori K, et al. Precursors to invasive pancreatic cancer. Adv Anat Pathol 2005;12:81–91.
3. Allen PJ. The management of intraductal papillary mucinous neoplasms of the pancreas. Surg Oncol Clin N Am 2010;19:297–310.
4. Allen PJ. The diagnosis and management of cystic lesions of the pancreas. Chin Clin Oncol 2017;6:60.
5. Tanaka M, Fernández-Del Castillo C, Kamisawa T, et al. Revisions of international consensus Fukuoka guidelines for the management of IPMN of the pancreas. Pancreatology 2017;17:738–753.
6. European Study Group on Cystic Tumours of the Pancreas. European evidence-based guidelines on pancreatic cystic neoplasms. Gut 2018;67:789–804.
7. Buscail E, Cauvin T, Fernandez B, et al. Intraductal papillary mucinous neoplasms of the pancreas and European guidelines: importance of the surgery type in the decision-making process. BMC Surg 2019;19:115.
8. **Springer S, Masica DL, Dal Molin M**, et al. A multimodality test to guide the management of patients with a pancreatic cyst. Sci Transl Med 2019;11:eaav4772.
9. Pergolini I, Sahora K, Ferrone CR, et al. Long-term risk of pancreatic malignancy in patients with branch duct intraductal papillary mucinous neoplasm in a referral center. Gastroenterology 2017;153:1284–1294.e1.
10. Kromrey ML, Bülow R, Hübner J, et al. Prospective study on the incidence, prevalence and 5-year pancreatic-related mortality of pancreatic cysts in a population-based study. Gut 2018;67:138–145.
11. Lobb RJ, Becker M, Wen SW, et al. Optimized exosome isolation protocol for cell culture supernatant and human plasma. J Extracell Vesicles 2015;4:27031.
12. Robin X, Turck N, Hainard A, et al. pROC: an open-source package for R and S+ to analyze and compare ROC curves. BMC Bioinformatics 2011;12:77.
13. **Lee K, Fraser K**, Ghaddar B, et al. Multiplexed profiling of single extracellular vesicles. ACS Nano 2018;12:494–503.
14. Görgens A, Bremer M, Ferrer-Tur R, et al. Optimisation of imaging flow cytometry for the analysis of single extracellular vesicles by using fluorescence-tagged vesicles as biological reference material. J Extracell Vesicles 2019;8:1587567.
15. Ko J, Wang Y, Gungabeesoon J, et al. Droplet-based single EV sequencing for rare immune subtype discovery. μ-TAS 2019 2019;T104c:85.
16. Akama K, Shirai K, Suzuki S. Droplet-free digital enzyme-linked immunosorbent assay based on a tyramide signal amplification system. Anal Chem 2016;88:7123–7129.
17. Furukawa T, Klöppel G, Volkan Adsay N, et al. Classification of types of intraductal papillary-mucinous neoplasm of the pancreas: a consensus study. Virchows Arch 2005;447:794–799.
18. Maker AV, Katabi N, Gonen M, et al. Pancreatic cyst fluid and serum mucin levels predict dysplasia in intraductal papillary mucinous neoplasms of the pancreas. Ann Surg Oncol 2011;18:199–206.

19. Gbormittah FO, Haab BB, Partyka K, et al. Characterization of glycoproteins in pancreatic cyst fluid using a high-performance multiple lectin affinity chromatography platform. J Proteome Res 2014;13:289–299.
20. Liu H, Shi J, Anandan V, et al. Reevaluation and identification of the best immunohistochemical panel (pVHL, Maspin, S100P, IMP-3) for ductal adenocarcinoma of the pancreas. Arch Pathol Lab Med 2012; 136:601–609.
21. Kaur S, Smith LM, Patel A, et al. A combination of MUC5AC and CA19-9 improves the diagnosis of pancreatic cancer: a multicenter study. Am J Gastroenterol 2017;112:172–183.
22. Sinha J, Cao Z, Dai J, et al. A gastric glycoform of MUC5AC is a biomarker of mucinous cysts of the pancreas. PLoS One 2016;11:e0167070.
23. Basturk O, Khayyata S, Klimstra DS, et al. Preferential expression of MUC6 in oncocytic and pancreatobiliary types of intraductal papillary neoplasms highlights a pyloropancreatic pathway, distinct from the intestinal pathway, in pancreatic carcinogenesis. Am J Surg Pathol 2010;34:364–370.
24. Das KK, Xiao H, Geng X, et al. mAb Das-1 is specific for high-risk and malignant intraductal papillary mucinous neoplasm (IPMN). Gut 2014;63:1626–1634.
25. Das KK, Geng X, Brown JW, et al. Cross validation of the monoclonal antibody Das-1 in identification of high-risk mucinous pancreatic cystic lesions. Gastroenterology 2019;157:720–730.e2.
26. Okada K, Hirabayashi K, Imaizumi T, et al. Stromal thrombospondin-1 expression is a prognostic indicator and a new marker of invasiveness in intraductal papillary-mucinous neoplasm of the pancreas. Biomed Res 2010;31:13–19.
27. Tobita K, Kijima H, Dowaki S, et al. Thrombospondin-1 expression as a prognostic predictor of pancreatic ductal carcinoma. Int J Oncol 2002;21:1189–1195.
28. Kim J, Bamlet WR, Oberg AL, et al. Detection of early pancreatic ductal adenocarcinoma with thrombospondin-2 and CA19-9 blood markers. Sci Transl Med 2017;9:eaah5583.
29. Jabbar KS, Arike L, Verbeke CS, et al. Highly accurate identification of cystic precursor lesions of pancreatic cancer through targeted mass spectrometry: a phase IIc diagnostic study. J Clin Oncol 2018;36:367–375.
30. Bausch D, Mino-Kenudson M, Fernández-Del Castillo C, et al. Plectin-1 is a biomarker of malignant pancreatic intraductal papillary mucinous neoplasms. J Gastrointest Surg 2009;13:1948–1954; discussion: 1954.
31. Chen R, Yi EC, Donohoe S, et al. Pancreatic cancer proteome: the proteins that underlie invasion, metastasis, and immunologic escape. Gastroenterology 2005; 129:1187–1197.
32. Jang JY, Park YC, Song YS, et al. Increased K-ras mutation and expression of S100A4 and MUC2 protein in the malignant intraductal papillary mucinous tumor of the pancreas. J Hepatobiliary Pancreat Surg 2009;16:668–674.
33. Suzuki K, Watanabe A, Araki K, et al. High STMN1 expression is associated with tumor differentiation and metastasis in clinical patients with pancreatic cancer. Anticancer Res 2018;38:939–944.
34. Watanabe A, Araki K, Yokobori T, et al. Stathmin 1 promotes the proliferation and malignant transformation of pancreatic intraductal papillary mucinous neoplasms. Oncol Lett 2017;13:1783–1788.
35. **Do M, Han D**, Wang JI, et al. Quantitative proteomic analysis of pancreatic cyst fluid proteins associated with malignancy in intraductal papillary mucinous neoplasms. Clin Proteomics 2018;15:17.
36. **Springer S, Wang Y, Dal Molin M**, et al. A combination of molecular markers and clinical features improve the classification of pancreatic cysts. Gastroenterology 2015;149:1501–1510.
37. Cancer Genome Atlas Research Network. Integrated genomic characterization of pancreatic ductal adenocarcinoma. Cancer Cell 2017;32:185–203.e13.
38. Mito K, Saito M, Morita K, et al. Clinicopathological and prognostic significance of MUC13 and AGR2 expression in intraductal papillary mucinous neoplasms of the pancreas. Pancreatology 2018;18:407–412.
39. Stiles ZE, Khan S, Patton KT, et al. Transmembrane mucin MUC13 distinguishes intraductal papillary mucinous neoplasms from non-mucinous cysts and is associated with high-risk lesions. HPB (Oxford) 2019;21:87–95.
40. Lahat G, Lubezky N, Loewenstein S, et al. Epithelial-to-mesenchymal transition (EMT) in intraductal papillary mucinous neoplasm (IPMN) is associated with high tumor grade and adverse outcomes. Ann Surg Oncol 2014; 21(Suppl 4):S750–S757.
41. **Chang YR, Park T**, Park SH, et al. Prognostic significance of E-cadherin and ZEB1 expression in intraductal papillary mucinous neoplasm. Oncotarget 2018;9:306–320.
42. Kanno A, Satoh K, Kimura K, et al. The expression of MUC4 and MUC5AC is related to the biologic malignancy of intraductal papillary mucinous neoplasms of the pancreas. Pancreas 2006;33:391–396.
43. **Melo SA, Luecke LB, Kahlert C**, et al. Glypican-1 identifies cancer exosomes and detects early pancreatic cancer. Nature 2015;523:177–182.
44. **Frampton AE, Prado MM**, López-Jiménez E, et al. Glypican-1 is enriched in circulating-exosomes in pancreatic cancer and correlates with tumor burden. Oncotarget 2018;9:19006–19013.
45. Tanaka M, Ishikawa S, Ushiku T, et al. EVI1 modulates oncogenic role of GPC1 in pancreatic carcinogenesis. Oncotarget 2017;8:99552–99566.
46. Nie S, Lo A, Wu J, et al. Glycoprotein biomarker panel for pancreatic cancer discovered by quantitative proteomics analysis. J Proteome Res 2014;13:1873–1884.
47. **Jenkinson C, Elliott VL, Evans A**, et al. Decreased serum thrombospondin-1 levels in pancreatic cancer patients up to 24 months prior to clinical diagnosis: association with diabetes mellitus. Clin Cancer Res 2016; 22:1734–1743.
48. Kang HJ, Lee JM, Joo I, et al. Assessment of malignant potential in intraductal papillary mucinous neoplasms of the pancreas: comparison between multidetector CT and MR imaging with MR cholangiopancreatography. Radiology 2016;279:128–139.
49. Matsuda Y, Kimura W, Matsukawa M, et al. Association between pancreatic cystic lesions and high-grade

intraepithelial neoplasia and aging: an autopsy study. Pancreas 2019;48:1079–1085.
50. Cohen JD, Li L, Wang Y, et al. Detection and localization of surgically resectable cancers with a multi-analyte blood test. Science 2018;359:926–930.
51. Yang Y, Yan S, Tian H, et al. Macrophage inhibitory cytokine-1 versus carbohydrate antigen 19-9 as a biomarker for diagnosis of pancreatic cancer: a PRISMA-compliant meta-analysis of diagnostic accuracy studies. Medicine (Baltimore) 2018;97:e9994.
52. Pan S, Chen R, Crispin DA, et al. Protein alterations associated with pancreatic cancer and chronic pancreatitis found in human plasma using global quantitative proteomics profiling. J Proteome Res 2011;10:2359–2376.
53. **Yang KS, Im H, Hong S**, et al. Multiparametric plasma EV profiling facilitates diagnosis of pancreatic malignancy. Sci Transl Med 2017;9:eaal3226.
54. Zhang Y, Yang J, Li H, et al. Tumor markers CA19-9, CA242 and CEA in the diagnosis of pancreatic cancer: a meta-analysis. Int J Clin Exp Med 2015;8:11683–11691.
55. Tang H, Partyka K, Hsueh P, et al. Glycans related to the CA19-9 antigen are elevated in distinct subsets of pancreatic cancers and improve diagnostic accuracy over CA19-9. Cell Mol Gastroenterol Hepatol 2016;2:201–221.e15.
56. **Singh S, Pal K**, Yadav J, et al. Upregulation of glycans containing 3′ fucose in a subset of pancreatic cancers uncovered using fusion-tagged lectins. J Proteome Res 2015;14:2594–2605.
57. Ciprani D, Morales-Oyarvide V, Qadan M, et al. An elevated CA 19-9 is associated with invasive cancer and worse survival in IPMN. Pancreatology 2020;20:729–735.
58. Young MR, Wagner PD, Ghosh S, et al. Validation of biomarkers for early detection of pancreatic cancer: summary of the Alliance of Pancreatic Cancer Consortia for Biomarkers for Early Detection Workshop. Pancreas 2018;47:135–141.
59. **Scholten L, van Huijgevoort NCM**, Bruno MJ, et al. Surgical management of intraductal papillary mucinous neoplasm with main duct involvement: an international expert survey and case-vignette study. Surgery 2018;164:17–23.
60. Attiyeh MA, Fernández-Del Castillo C, Al Efishat M, et al. Development and validation of a multi-institutional preoperative nomogram for predicting grade of dysplasia in intraductal papillary mucinous neoplasms (IPMNs) of the pancreas: a report from the Pancreatic Surgery Consortium. Ann Surg 2018;267:157–163.
61. Shao H, Im H, Castro CM, et al. New technologies for analysis of extracellular vesicles. Chem Rev 2018;118:1917–1950.
62. Cohen L, Walt DR. Single-molecule arrays for protein and nucleic acid analysis. Annu Rev Anal Chem (Palo Alto Calif) 2017;10:345–363.
63. **Madhavan B, Yue S, Galli U**, et al. Combined evaluation of a panel of protein and miRNA serum-exosome biomarkers for pancreatic cancer diagnosis increases sensitivity and specificity. Int J Cancer 2015;136:2616–2627.
64. Liang K, Liu F, Fan J, et al. Nanoplasmonic quantification of tumor-derived extracellular vesicles in plasma microsamples for diagnosis and treatment monitoring. Nat Biomed Eng 2017;1:0021.
65. Ferguson S, Weissleder R. Modeling EV kinetics for use in early cancer detection. Adv Biosyst 2020;4:e1900305.
66. Aronsson L, Andersson R, Bauden M, et al. High-density and targeted glycoproteomic profiling of serum proteins in pancreatic cancer and intraductal papillary mucinous neoplasm. Scand J Gastroenterol 2018;53:1597–1603.
67. Wang Y, Sun Y, Feng J, et al. Glycopatterns and glycoproteins changes in MCN and SCN: a prospective cohort study. Biomed Res Int 2019;2019:2871289.
68. Park J, Han D, Do M, et al. Proteome characterization of human pancreatic cyst fluid from intraductal papillary mucinous neoplasm by liquid chromatography/tandem mass spectrometry. Rapid Commun Mass Spectrom 2017;31:1761–1772.

Author names in bold designate shared co-first authorship.

Received July 20, 2020. Accepted November 18, 2020.

Correspondence
Address correspondence to: R. Weissleder, MD, PhD, Center for Systems Biology, Massachusetts General Hospital, 185 Cambridge Street, CPZN 5206, Boston, Massachusetts 02114. e-mail: ralph_weissleder@hms.harvard.edu.

Acknowledgments
The authors thank Scott Ferguson, Hyungsoon Im, Xandra Breakefield, Hakho Lee, and Jonathan Carlson for helpful discussion and are grateful to Nidhi Shanakar and Alexandra Dibrindisi, who contributed to preliminary feasibility data.

CRediT Authorship Contributions
Katherine S. Yang, PhD (Data curation: Lead; Formal analysis: Lead; Investigation: Lead; Visualization: Lead; Writing – original draft: Equal; Writing – review & editing: Lead). Debora Ciprani, MD (Resources: Equal). Aileen O'Shea, MD (Resources: Supporting; Visualization: Supporting; Writing – review & editing: Supporting). Andrew Liss, PhD (Resources: Supporting). Robert Yang, PhD (Formal analysis: Supporting; Investigation: Equal; Visualization: Equal; Writing – review & editing: Supporting). Sarah Fletcher-Mercaldo, PhD (Formal analysis: Supporting). Mari Mino-Kenudson, MD (Resources: Supporting). Carlos Fernández-del Castillo, MD (Conceptualization: Supporting; Writing – review & editing: Supporting). Ralph Weissleder, MD, PhD (Funding acquisition: Lead; Supervision: Lead; Visualization: Supporting; Writing – original draft: Equal; Writing – review & editing: Equal).

Conflicts of interest
The authors disclose no conflicts.

Funding
This work was supported in part by the following National Institutes of Health grants from the National Cancer Institute: R01CA237332, R01CA204019, R21CA236561, and P01CA069246; by the Andrew L. Warshaw, MD Institute for Pancreatic Cancer Research; and by the William F. Milton Fund.

Supplementary Methods

Cell lines

AsPC-1, BxPC-3, MIA PaCa-2, and Capan-2 cell lines were purchased from the American Type Culture Collection (Manassas, VA). AsPC-1 and BxPC-3 cells were cultured in RPMI-1640 medium (11875119, Thermo Fisher Scientific). MIA Paca-2 cells were cultured in Dulbecco's modified Eagle medium (10-013-CV; Mediatech, Manassas, VA), and Capan-2 cells were cultured in McCoy's 5a medium (16600108, Thermo Fisher Scientific). All media were supplemented with 10% fetal bovine serum (S12450; Atlanta Biologicals, Flowery Branch, GA), 100 IU penicillin, and 100 μg/mL streptomycin (30-002-CI; Mediatech). PDAC (1531 and 1617) and IPMN (1505 and 1966) PDX cell lines were from the Massachusetts General Hospital pancreas biobank. Both PDX cell lines were maintained in a 50:50 mix of Ham's F-12 and Dulbecco's modified Eagle medium. PDAC PDX cells were supplemented as above. IPMN PDX cell lines were supplemented with 20% fetal bovine serum, 1% antibiotic-antimycotic (15240062; Thermo Fisher Scientific), 10 mmol/L nicotinamide (N0636; Sigma-Aldrich, St Louis, MO), 1X insulin-transferrin-selenium (25-800-CR; Corning), 8.4 ng/mL cholera toxin (C8052; Sigma-Aldrich,), 10 ng/mL epidermal growth factor (E9644; Sigma-Aldrich), and 10 ng/mL hepatocyte growth factor (PHG0324; Thermo Fisher Scientific).

Antibody-Bead Coupling and Biotinylation

Capture antibodies were coupled to Dynabeads M-270 Epoxy magnetic beads using a coupling kit (14311D, Thermo Fisher Scientific). All buffers used in the coupling reaction were provided in the kit (Buffers C1, C2, HB, LB, SB). Briefly, Dynabeads were weighed into Eppendorf tubes and washed once with Buffer C1. Antibody was added to beads at a ratio of 10 μg antibody/mg Dynabeads. Buffer C1 was added to the antibody solution for a total volume of 50 μL/mg bead. The total reaction volume (Buffer C1 + antibody + Buffer C2) was 100 μL/mg Dynabeads (manufacturer's instructions; 14311D, Thermo Fisher Scientific). The bead-antibody mixture was incubated overnight at 37°C on a HulaMixer (35 rpm, 5° tilt, 5° rotation; all 5 sec). The antibody solution was saved to determine coupling efficiency, and beads were then washed with Buffer HB and LB (containing 0.05% Tween-20), followed by 2 washes with Buffer SB.

Beads were then incubated in Buffer SB for 15 minutes, the solution was removed, and the final antibody-bead conjugate was stored at 4°C in 100 μL buffer SB/mg Dynabead. After each wash, beads were incubated 1 minute on a DynaMag magnet, and wash buffer was discarded. Coupling efficiency was typically 20% to 80%, depending on the capture antibody. Detection antibodies that were not readily available as a biotinylated product were prepared using sulfo-NHS-LC-BIOTIN (A39257, Thermo Fisher Scientific). Briefly, a 20-fold molar excess of biotin was calculated for 50 μg of antibody. Then, 180 μL of ultrapure water was added to a 1-mg no-weigh vial of biotin to make a 10 mmol/L stock solution. An appropriate volume of biotin was added to the antibody in PBS and incubated for 30 minutes at room temperature. Excess biotin was then removed using a 0.5 mL, 7MWCO Zeba column (89882, Thermo Fisher Scientific), according to the manufacturers' instructions. Final biotinylated antibody concentrations were determined using a Nanodrop (ND-1000, Thermo Fisher Scientific).

Supplementary Reference

1. Pergolini I, Morales-Oyarvide V, Mino-Kenudson M, et al. Tumor engraftment in patient-derived xenografts of pancreatic ductal adenocarcinoma is associated with adverse clinicopathological features and poor survival. PLoS One 2017;12:e0182855.

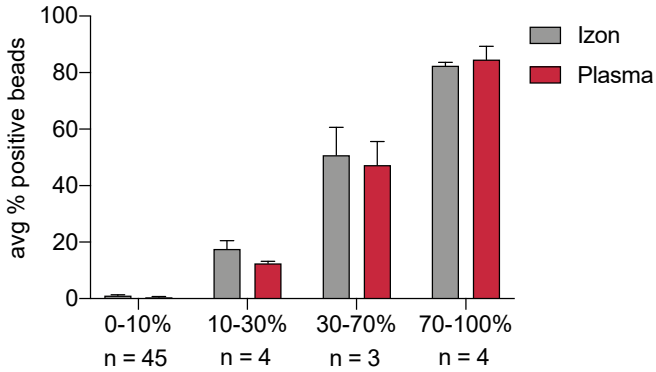

Supplementary Figure 1. Effect of EV isolation on MUC5AC measurements. Plasma EVs were isolated by Izon column separation or direct processing. The direct method (DEST) is a combination of immunobead enrichment, coupled with washing and lowering backgrounds by dual antibody capture (see Figure 1). MUC5AC analysis in EVs was done using Izon column purification or the DEST method in unpurified plasma. Note the congruence of the methods. We settled on using the direct DEST method because there is no loss of EVs, it is fast, and does not change the make-up of EV populations. The *error bars* represent the standard error of the mean.

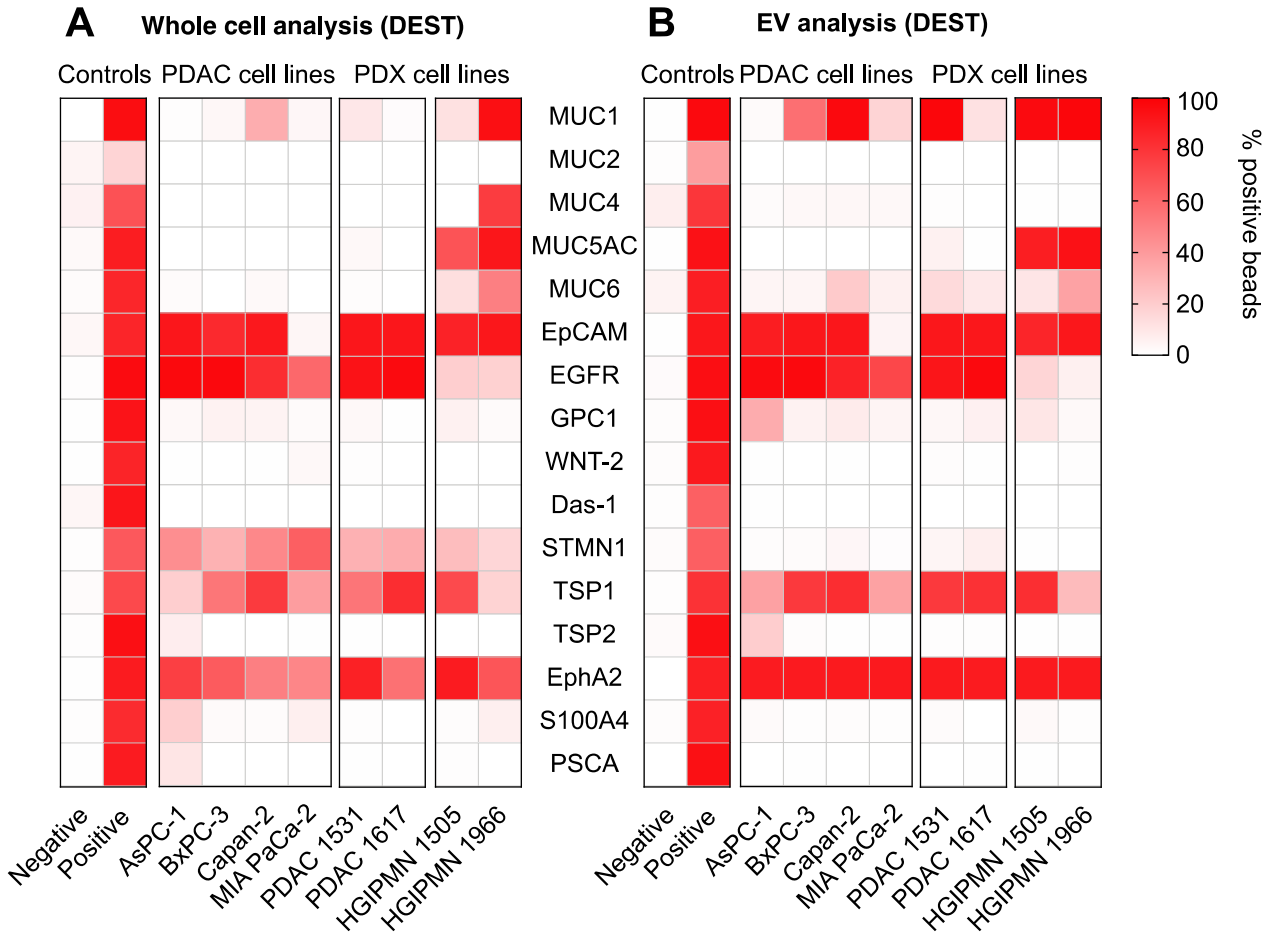

Supplementary Figure 2. Characterization of molecular targets on IPMN and PDAC cell lines and their derived EVs. (*A*) Four PDAC cell lines (ASPC-1, BxPC-3, Capan-2, and MIA PaCa-2), 2 PDAC PDX (PDAC1531, PDAC1617),[1] and 2 invasive HG-IPMN PDX (HGIPMN 1505, HGIPMN1966) were analyzed for the presence or absence of 16 molecular markers. Controls refer to antibody testing against isolated proteins or known positive EV lysates. (*B*) DEST analysis of EV fractions obtained from the same cell lines shows presence of certain molecular targets from parental cells. Note that EV targets were only detected when also present in parental cells. Furthermore, MUC5AC was elevated in both HG-IPMN PDX models.

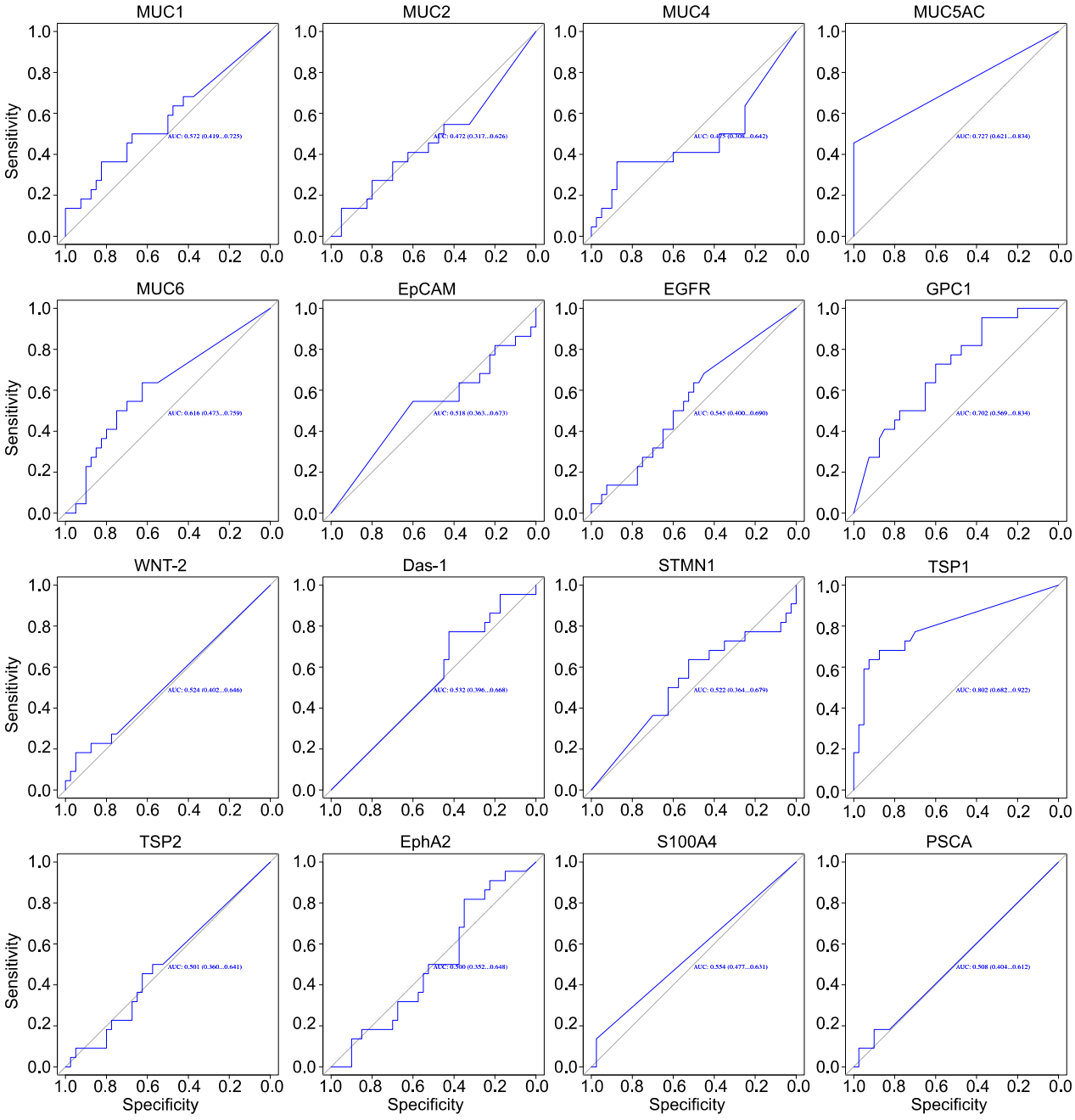

Supplementary Figure 3. ROC curve analysis for the different EV biomarkers in the discovery cohort. AUC (95% confidence interval) analysis for LG-IPMN vs HG-IPMN. Note that MUC2, MUC4, GPC1, EpCAM, Das-1, STMN1, and TSP2 are slightly better positive predictors of LG-IPMN. All other markers are positive predictors of HG-IPMN.

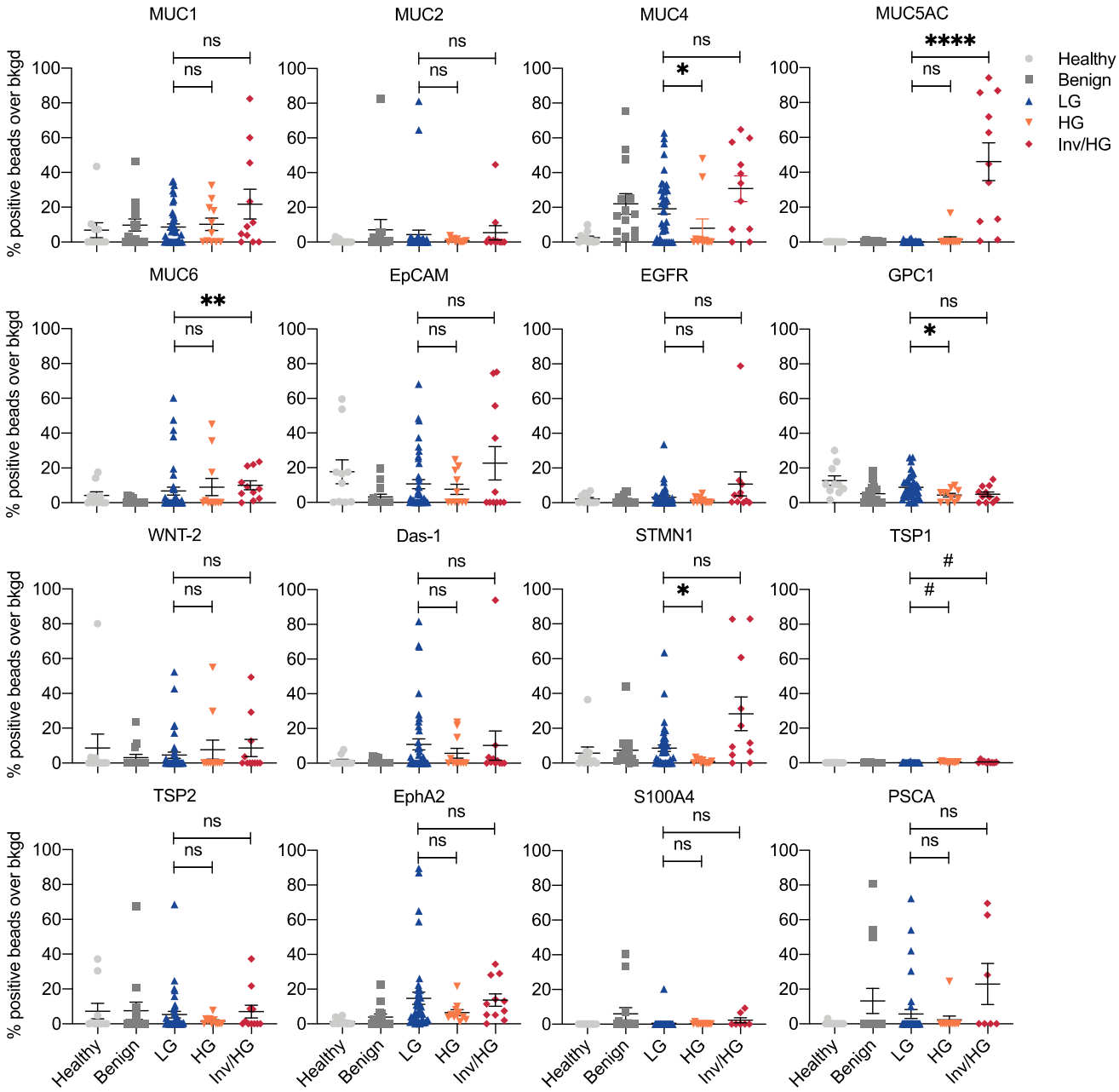

Supplementary Figure 4. Analysis of 16 prototypical biomarkers in EV from different discovery cohort patient subgroups. Each data point represents an EV sample from a single patient. Data shown are from healthy controls (n = 10); benign (age-matched control patients undergoing abdominal surgery but without evidence for any pancreatic lesions; n = 14 patients); LG-IPMN (n = 40 patients); HG-IPMN (n = 11 patients), and Inv/HG-IPMN (n = 11 patients). See Table 1 for patient demographics. Differences between HG-IPMN and LG-IPMN: ****$P < .0001$, **$P < .01$; *$P < .05$, ns = not statistically significant ($P > .05$); #TSP1 is statistically significant but the extremely low signal over background makes the results clinically unreliable. The *error bars* represent the standard error of the mean.

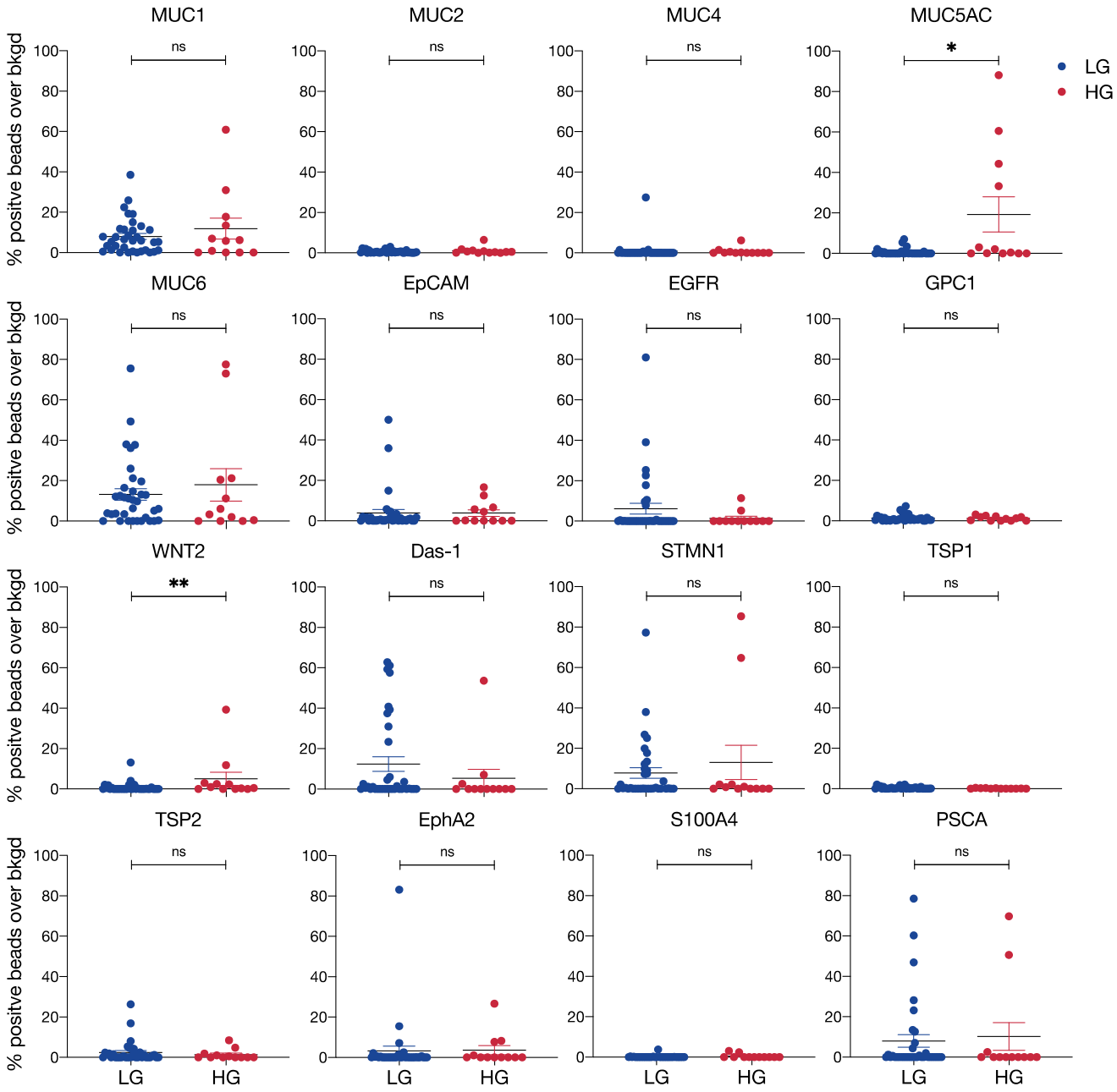

Supplementary Figure 5. Analysis of 16 biomarkers in EV from validation cohort LG-IPMN and HG-IPMN lesions. Each data point represents an EV sample from a single patient. Data shown are from LG- IPMN (n = 35) and HG-IPMN (n = 12). See Table 1 for cohort demographics. Differences between HG-IPMN and LG-IPMN: $^{**}P < .01$; $^{*}P < .05$; ns = not statistically significant ($P > .05$).

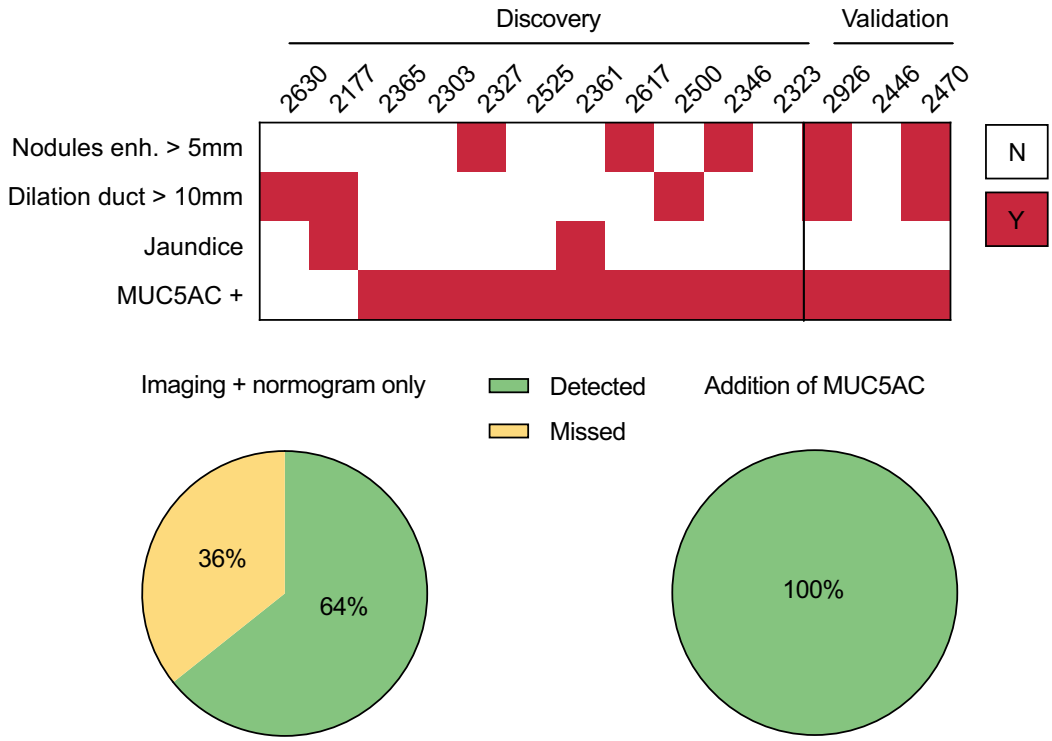

Supplementary Figure 6. Biomarkers for the decision to surgically remove HG-IPMN. In the 14 patients with inv/HG-IPMN traditional imaging and high-risk stigmata alone would have missed 5 of the 14 patients requiring surgery (36% miss rate). If MUC5AC EV testing was added, all patients requiring immediate surgery would have been identified correctly.

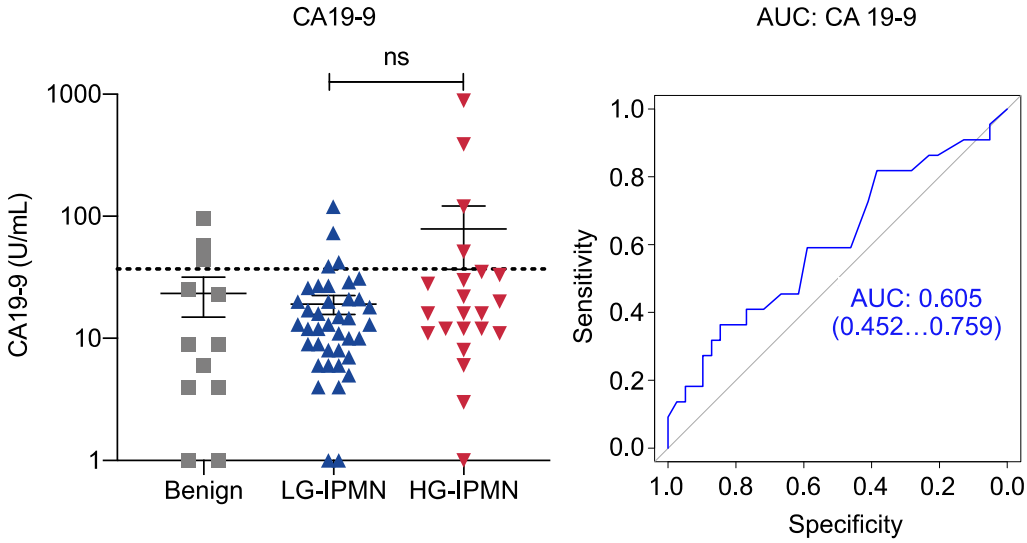

Supplementary Figure 7. Value of CA19-9 measurement in IPMN. Plasma levels of CA19-9 are not statistically different between the different groups, and the AUC (95% confidence interval) is 0.6, indicating poor discriminatory capabilities. ns = not significant ($P > .05$).

Supplementary Table 1. Experimental Details of Digital Extracellular Vesicle Screening Technique Assay

Step	Reagent	Time (*min*)	Volume (μL)	Concentration	Buffer
1	Blocking	30	100	1.5μL (~1 million) beads/well	Antibody dependent, see Supplementary Table 4
2	Wash	4 washes	100	—	PBS + 0.1% Tween-20
3	Incubation with sample	60	100	1–10 μL plasma, 250 ng EVs or cell lysate controls	Blocking buffer
4	Wash	4 washes	100	…	PBS + 0.1% Tween-20
5	Detection antibody	60	50	0.5 μg/mL	Blocking buffer
6	Wash	4 washes	100	…	PBS + 0.1% Tween-20
7	Streptavidin-HRP	30	100	137.5 ng/mL	Blocking buffer + 0.1% Tween-20
8	Wash	4 washes	100	…	PBS + 0.1% Tween-20
9	Biotin tyramide (signal amplification)	10	100	5 μg/mL	0.1 mol/L Borate buffer (pH 8.5) + 0.003% H_2O_2
10	Wash	4 washes	100	…	PBS + 0.1% Tween-20
11	Brilliant violet 421 streptavidin	30	50	0.5 μg/mL	Blocking buffer
12	Wash	4 washes	100	…	PBS + 0.1% Tween-20
Total		220 min			

NOTE. Each initial plasma EV sample is 1 or 10 μL. Beads are collected using a 96-well plate magnet for each wash step. Each incubation step is done on a plate shaker to maintain beads in suspension. MUC1 and MUC5AC were incubated in human anti-mouse antibody blocker in step 3.
HRP, horseradish peroxidase.

Supplementary Table 2. List of Reagents Used in the Digital Extracellular Vesicle Screening Technique Assay

Reagent	Company	Catalog #	Concentration	
			Stock	Final
Bovine serum albumin	Fisher Scientific	BP1605–100	…	2% w/v
UltraBlock	Bio-Rad	BUF033C	…	Use neat
HAMA Blocker	Abcam	ab193969	…	Use neat
PBS	Thermo Scientific	70011069	10X	1X
Tween-20	Sigma-Aldrich	P9416–100 mL	100%	0.1%
Pooled normal human plasma (K2 EDTA)	Innovative Research Inc.	IPLA-N	…	1–10 μL
Streptavidin-HRP	Thermo Scientific	21130	1.1mg/mL	137.5 ng/mL
Biotinyl tyramide	Sigma-Aldrich	SML2135–50 mg	2 mg/mL (DMSO)	5 μg/mL
Boric acid	Sigma-Aldrich	B6768–500 g	—	0.1 mol/L, pH 8.5
Hydrogen peroxide solution	Sigma-Aldrich	H1009–100 mL	30%	0.003%
Brilliant violet 421 streptavidin	BioLegend	405225	0.5 mg/mL	0.5 μg/mL

DMSO, dimethyl sulfoxide; HAMA, human anti-mouse antibody; HRP, horseradish peroxidase; w/v, weight/volume.
Supplementary Table 3. Antibodies Used in This Study
Polyclonal antibodies. All other antibodies are monoclonal

Supplementary Table 4. Digital Extracellular Vesicle Screening Technique Antibody Pair Conditions and Controls

Target	Blocking	Vol. plasma	Negative ctrl	Positive ctrl
MUC1	2% BSA/HAMA	1 μL	Daudi EV[a]	Capan-2 EV[a]
MUC2	2% BSA	10 μL	Daudi EV[a]	1966 cell
MUC4	2% BSA	10 μL	Daudi EV[a]	1966 cell
MUC5AC	UltraBlock/HAMA	10 μL	1617 EV	1505 EV
MUC6	2% BSA	10 μL	Daudi EV[a]	1966 cell
EpCAM	2% BSA	10 μL	Daudi EV[a]	1617 EV
EGFR	2% BSA	10 μL	Daudi EV[a]	BxPC3 cell
GPC1	2% BSA	1 μL	Daudi EV[a]	GPC1 protein
WNT2	2% BSA	1 μL	Daudi EV[a]	WNT2 protein
Das-1	UltraBlock	10 μL	1617 EV	LS180 EV
STMN1	2% BSA	10 μL	1617 EV	Mia PaCa-2 cell
TSP1	UltraBlock	1 μL	Daudi EV[a]	TSP1 protein
TSP2	2% BSA	1 μL	1617 EV	TSP2 protein
EphA2	2% BSA	10 μL	Daudi EV[a]	A549 EV[a]
S100A4	2% BSA	10 μL	Daudi EV[a]	S100A4 protein
PSCA	2% BSA	10 μL	Daudi EV[a]	PSCA protein

NOTE. Blocking buffers used for each antibody pair, plasma volume, and negative and positive controls.
BSA, bovine serum albumin; HAMA, human anti-mouse antibody.
[a]Control confirmed for corresponding cell line in the Human Protein Atlas database.

Supplementary Table 5. Additional Antibodies Tested, but Found to be Unsuitable for Digital Extracellular Vesicle Screening Technique

	Alternative antibodies tested
Target	Vendor (Cat No.)
MUC1	Fitzgerald (10-M93A), BioLegend (355602)
MUC2	Antibodies-online (ABIN1173448), Novus (H000-4583-M02, NBP2-25221)
MUC5AC	Novus (NBP2-44452, NBP2-15196, H00004586-M07, NBP2-44458)
MUC6	Origene (TA322537), Novus (NBP2-44376)
EGFR	Sino Biological Inc (10001-RE11, 10001-R021), R&D (BAF231)
EpCAM	BioLegend (324215), Thermo (710524), Abcam (ab20160)
WNT2	R&D (AF3464), Novus (2295002), Santa Cruz (sc-514382)
PSCA	Fitzgerald (70R-19568), Novus (H00008000-M02)
TSP1	Thermo (MA5-13395)
MUC13	Sigma (SAB4502427), Fitzgerald (70R-32134)
ZEB1	Origene (TA590279), Novus (NBP2-37329)
PLEC1	Abcam (ab32528), Santa Cruz (sc-33649), Origene (TA351536), Millipore (MAB5674)
HOOK1	Novus (H00051361-AP21, antibody pair)
PTPN6	Novus (H00005777-AP22, antibody pair)
FBN1	Millipore (MAB2499, MAB2502)

Supplementary Table 6. Extracellular Vesicle Biomarker Analysis in the Validation Cohort

	Invasive HG-IPMN				Noninvasive HG-IPMN				Combined HG-IPMN			
Biomarker(s)	Sensitivity	Specificity	F1	PPV	Sensitivity	Specificity	F1	PPV	Sensitivity	Specificity	F1	PPV
MUC5AC	1.00 (1.00–1.00)	1.00 (1.00–1.00)	1.00	1.00	0.11 (0.00–0.33)	1.0 (1.00–1.00)	0.20	1.00	0.33 (0.08–0.58)	0.97 (0.91–1.00)	0.47	0.80
Imaging alone	0.33 (0.00–1.00)	0.94 (0.86–1.00)	0.33	0.33	0.67 (0.33–0.89)	0.94 (0.86–1.00)	0.71	0.75	0.58 (0.33–0.83)	0.94 (0.86–1.00)	0.67	0.80
DEST + Imaging	1.00 (1.00–1.00)	0.94 (0/86–1.00)	1.00	0.60	0.67 (0.33–0.89)	0.89 (0.77–0.97)	0.63	0.60	0.75 (0.50–1.00)	0.89 (0.77–0.97)	0.72	0.69

NOTE. All numbers for sensitivity, specificity, F1 score, and positive predictive value (PPV) are in fractions and are compared with LG-IPMN. The 95% confidence intervals of this small series are shown in parentheses.